Thin–Walled Structures 154 (2020) 106875

Contents lists available at ScienceDirect

Thin-Walled Structures

journal homepage: http://www.elsevier.com/locate/tws

Full length article

Investigation of different steel intermediate moment frame connections under column-loss scenario

Mohammed Alrubaidi, Hussein Elsanadedy, Husain Abbas, Tarek Almusallam, Yousef Al-Salloum *

Chair of Research and Studies in Strengthening and Rehabilitation of Structures, Dept. of Civil Engineering, College of Engineering, King Saud University, P.O. Box 800, Riyadh, 11421, Saudi Arabia

ARTICLE INFO

Keywords:
Progressive collapse
Steel beam-column connection
Column removal scenario
Catenary action
Intermediate moment frames
FE

ABSTRACT

This paper investigated experimentally the progressive collapse risk of three one-third scale single story, two-bay steel frames under column-loss event. Progressive collapse was simulated by applying a vertical loading on the middle column. In these tests, three different types of steel beam-to-column connections were studied. These included: one shear-connection specimen that signified the prevalent type of steel beam-column joints, and two different steel intermediate moment frame (IMF) connections conforming to ANSI/AISC 358–16. The three tested specimens along with another two 2D steel frames with IMF connection, tested in the literature, were used to calibrate 3D finite element (FE) models prepared using ABAQUS software. The validated FE models were then employed to investigate the risk of progressive collapse for eleven different types of steel IMF beam-column joints under middle column-loss scenario. Out of the eleven specimens, eight connections were designed as per ANSI/AISC 358–16; two joints were in accordance with EN 1993-Eurocode 3 and the last connection was in conformance with the 2007 Turkish-Earthquake Code (TEC-2007). Performance of different IMF connections was compared based on their modes of failure and load-displacement response in both flexural and catenary action stages.

1. Introduction

The vulnerability of strategic and critical infrastructure of the world to blast loads due to the terrorist threats is increasing at an alarming rate. As a result, engineers have highlighted a number of concerns regarding the risk of these structures under such terrorist related incidents.

Multi-story steel frame buildings are subjected during their service life to various types of actions arising from operation conditions. The design shall therefore provide an adequate structural resistance and durability to the structure to sustain these actions. Due to the uncertainties in occupancy or environmental loads but also due to other unforeseen hazards not explicitly considered in the design (accidental actions, e.g. fire, blast, gas explosion, or impact), the structure can be at risk of local damage. In turn, the local damage can lead to a spread of failure to neighboring elements and, in the end, to the collapse of excessively large part of the structure (or a complete collapse), known as progressive collapse. Several buildings have collapsed in this fashion such as the Ronan Point in U.K. due to a gas explosion in 1968 [1,2], Hotel New World in Singapore in 1986, Alfred P. Murrah Federal Building due to bombing in 1995 [3], and the World Trade Center in 2001 [4–7].

Marjanishvili and Agnew [8] presented methods that can be employed to carry out analysis to simulate progressive collapse (Nonlinear Dynamic; Linear Dynamic; Nonlinear Static; Linear Static) using SAP2000 software. Fu [9] analyzed a 20-story building using nonlinear dynamic approach and concluded that the columns directly connected to the removed column in the same floor need to be designed for axial load of twice the static axial load obtained for dead load plus 25% of the live load. Another major conclusion of the study was that the loss of column in upper stories would cause increase in vertical deflections as lesser number of stories contribute in resisting the progressive collapse. Steel-braced 10-story prototype buildings, designed for seismic loads, were numerically investigated by Khandelwal et al. [10] using alternate load path method in their dynamic analysis. The 2D macro-models of beam-column and discrete springs were employed to

* Corresponding author.
E-mail address: ysalloum@ksu.edu.sa (Y. Al-Salloum).

https://doi.org/10.1016/j.tws.2020.106875
Received 12 November 2019; Received in revised form 1 April 2020; Accepted 22 May 2020
Available online 13 June 2020
0263-8231/© 2020 Elsevier Ltd. All rights reserved.

Table 1
Details of specimens tested and used for FE validation[a].

Reference	Specimen ID	Column section $H \times B \times t_f \times t_w$ (mm)	Beam section $H \times B \times t_f \times t_w$ (mm)	Bolt	Size of shear plate/end plate (mm)	Connection type
Current study	*S*–C	H 200 × 200 × 12 × 8	H 194 × 150 × 9 × 6	Grade 10.9 M16	120 × 100 × 6	Shear
	WUF-FW	H 200 × 200 × 12 × 8	H 194 × 150 × 9 × 6	Grade 10.9 M16	120 × 100 × 6	IMF
	4 E-BUEEP-P	H 200 × 200 × 12 × 8	H 194 × 150 × 9 × 6	Grade 10.9 M20	356 × 170 × 12	IMF
Study of Dinu et al. [36]	CWP	IPE 260 × 260 × 17.5 × 10	IPE 220 × 110 × 9.2 × 5.9	Grade 8.8 M20	140 × 100 × 10	IMF
Study of Dinu et al. [36]	EPH	IPE 260 × 260 × 17.5 × 10	IPE 220 × 110 × 9.2 × 5.9	Grade 10.9 M20	460 × 130 × 20	IMF

[a] H = section depth; B = section width; t_f = thickness of section flange; t_w = thickness of section web; IMF = intermediate moment frame.

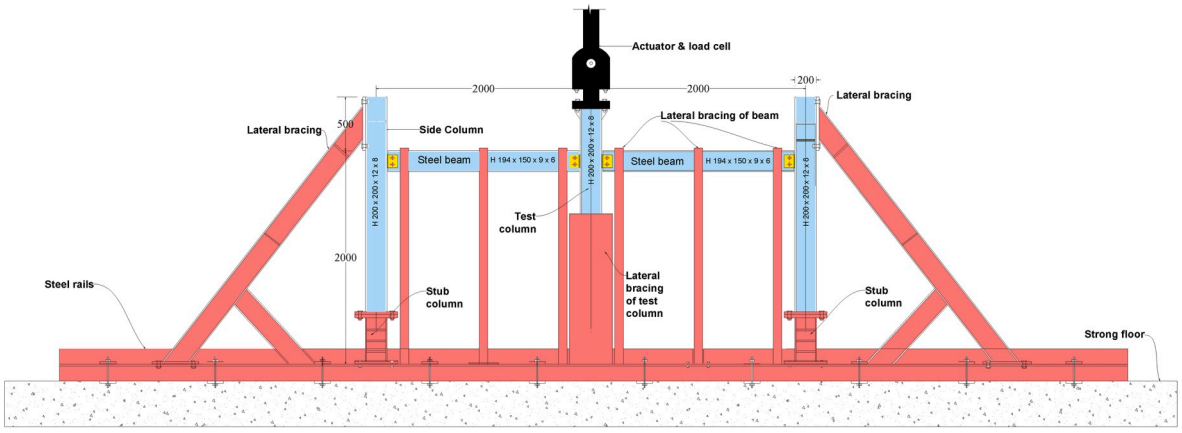

(a)

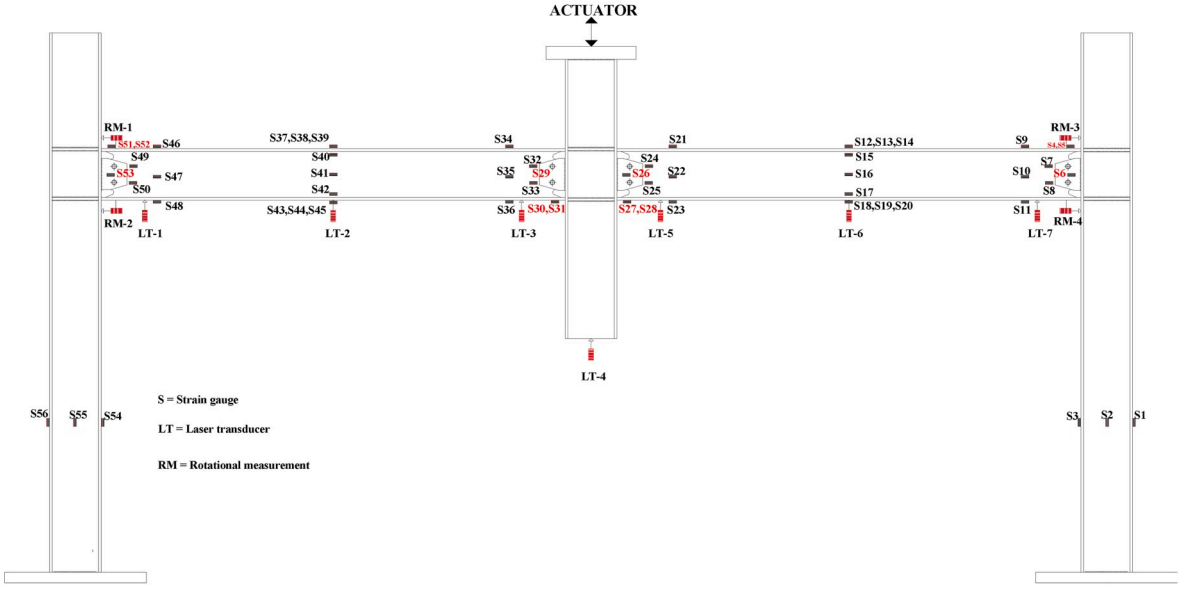

(b)

Fig. 1. Test setup and instrumentation layout: (a) Test setup; (b) Sensor locations for WUF-FW (Note: All dimensions are in mm).

simulate the structural response.

Progressive collapse of moment resisting steel frames was also studied by Kim and Kim [11]. The authors found that the linear static analysis would give lower structural response as compared to the results of nonlinear dynamic analysis. The analysis results showed considerable variation for different positions of removed column, applied load, or number of stories. Nevertheless, the linear static method was found to provide a relatively more conservative estimate.

Kim and An [12] carried out nonlinear static push-down analysis of steel moment frames to study the effect of the catenary action in resisting the progressive collapse. The results of analysis revealed the increase in the number of bays and stories increases the resistance of the structure against progressive collapse. Grierson et al. [13] used equivalent spring method to model the reduced stiffness in the linear static

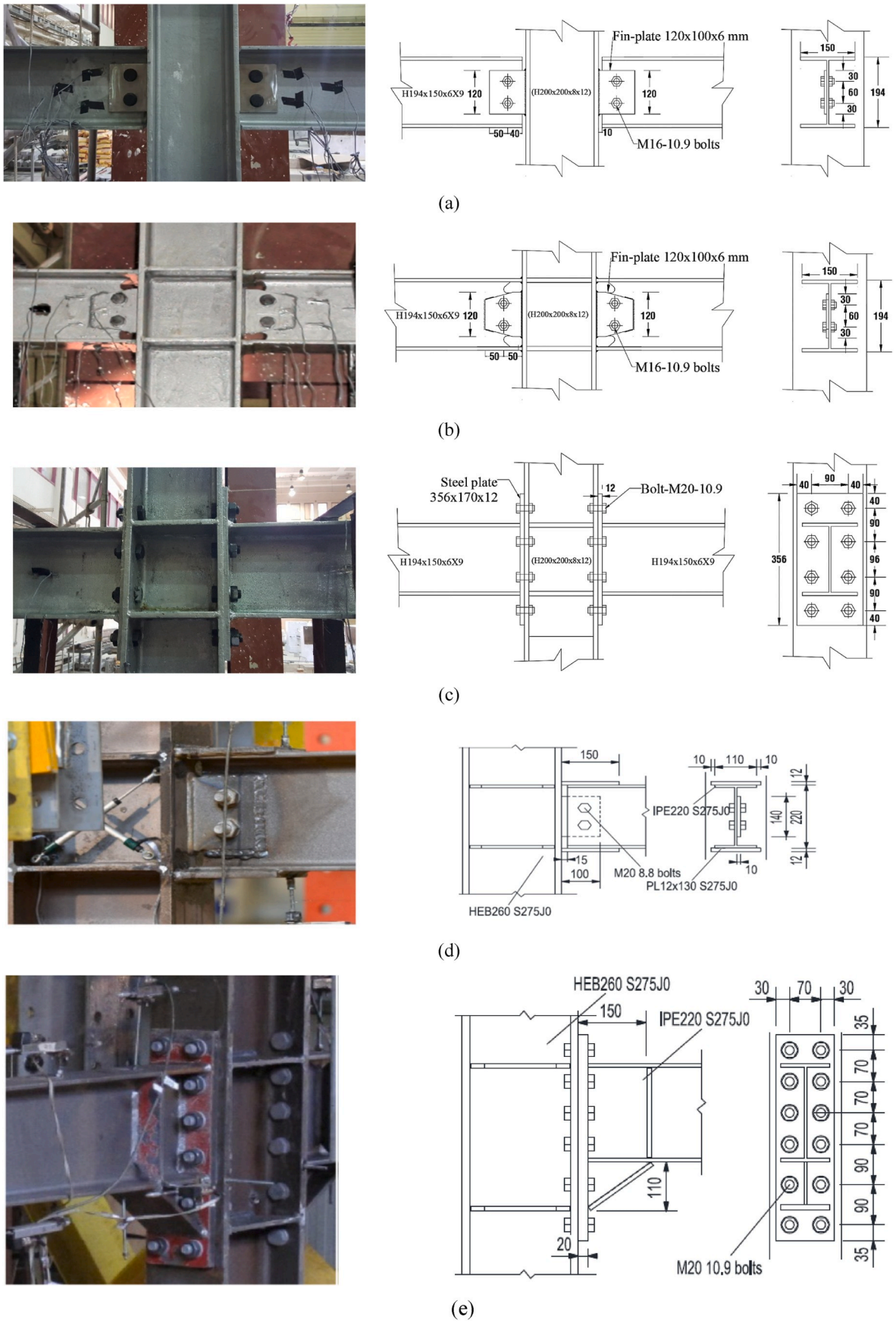

Fig. 2. Details of middle joint of specimens used for FE validation (Note: All dimensions are in mm): (a) Specimen *S*–C of current study; (b) Specimen WUF-FW of current study; (c) Specimen 4 E-BUEEP-P of current study; (d) Specimen CWP tested by Dinu et al. [36]; (e) Specimen EPH tested by Dinu et al. [36].

Table 2
Material properties of different components of specimens tested in current study.

Components	Elastic modulus E (GPa)	Yield strength f_y (MPa)	Tensile strength f_u (MPa)	Elongation at maximum stress δ_{ms} (%)	Elongation at fracture δ_f (%)
Column flange	205	295	466	16	22
Column web	212	304	462	14	20
Beam flange	194	332	471	15	23
Beam web	196	362	471	15	19
Shear plate	194	283	356	14	23
End plate	194	280	431	12	18
Bolt class 10.9	210	957	1071	–	10.3

progressive collapse analysis of steel framed building.

A simple approach was offered by Izzuddin et al. [14] and Vlassis et al. [15] for carrying out the nonlinear static progressive collapse analysis of steel framed buildings. A simple trilinear model was also developed by Lee et al. [16] to predict the vertical resistance in terms of the chord rotation of the double span beam (because of the removal of a column) for beam span-to-depth ratios of 10, 15, and 20. The developed model relies on the beam dimensions (span and cross-section). For other values of beam span-to-depth ratio, linear interpolation was proposed.

Naji and Irani [17] employed the capacity curve and load displacement response of a fixed beam to simplify the progressive collapse analysis procedure for steel framed buildings. The results of analysis were close to the results of nonlinear dynamic analysis. Elsanadedy et al. [18] performed progressive collapse analysis of a representative multi-story steel building against different blast cases using LS-DYNA software [19]. The published test results of steel tube exposed to blast load were used for the validation of numerical model.

Recently, Hadidi et al. [20] showed that steel frames, which are designed solely considering the seismic design specifications of AISC-LRFD [21], cannot resist progressive collapse, in terms of UFC requirements [22]. Mirtaheri and Zoghi [23] demonstrated that the progressive collapse vulnerability of a steel framed building depends on the column loss scenario and the type of analysis. Zoghi and Mirtaheri [24] presented 3D nonlinear dynamic (NLD) analysis for the progressive collapse assessment of an existing seismically code-designed steel building considering the effect of infill wall panels. The results showed that modeling the infill panels as well as the slabs can enhance the stability and catenary action of the building. Chen et al. [25] employed the energy principle to study the progressive collapse risk of steel moment framed buildings. Authors proposed a beam damage model with plastic hinges for analyzing the energy absorption during catenary action in beams. They also introduced a damage index to assess the occurrence of progressive collapse in steel framed buildings. Some researchers [26,27] have shown that the interaction between the axial force and flexure in plastic hinges and other regions has large reserve strength due to the strain hardening behavior of beam section, which is normally ignored in elastic-plastic analysis.

Bae et al. [28] studied different scenarios of progressive collapse in a steel framed building. The removal of corner columns was found to be critical for the partial progressive collapse of the building. Han et al. [29] employed macromodel to study the progressive collapse resistance of steel moment frames having stiffened beam-column connections. The model was capable of simulating the deformation of joints and the development of catenary action during progressive collapse. A dynamic magnification factor of 1.6 was recommended for the progressive analysis of connections used in the study.

Lew et al. [30] tested two full-scale steel beam-column assemblies under a central-column-loss scenario. The first assembly had a welded unreinforced flange and bolted web connections while the second one had reduced beam-section connections. The test results showed that the rotational capacities of both connections under monotonic column displacement were approximately twice as large as those based on seismic test data. Gong [31] carried out similar tests on two types of beam-column connections: web-bolted angle and flange, and web-bolted angles. Tensile deformation and strength capacities of bolted angle connections were determined after testing 31 bolted-angle connections under pure tension.

Recent work has been published by Liu et al. [32] on experimental and numerical studies of the response of two-span beams, joined to a central column by web-cleat connections, when the column support is suddenly removed. This work shows good correlation between the experimental tests and the numerical model, but on a level related to the entire system rather than specifically concentrating on the connection performance.

It is worth mentioning that the beam-column connections play a critical role in the development of catenary action in a building frame due to the limited rotation capacity of the connections [33–36]. Design procedures for intermediate moment frame (IMF) connections [37–40] are often used in structural designs for mitigating progressive collapse. The main purpose of using IMF connections is for securing a low level of rotation capacity [36]. But there are several concerns to be addressed for avoiding localized failures under column-loss scenario [36]. Additional data on the progressive collapse response of different types of steel IMF connections in the event of losing one or more columns are therefore needed.

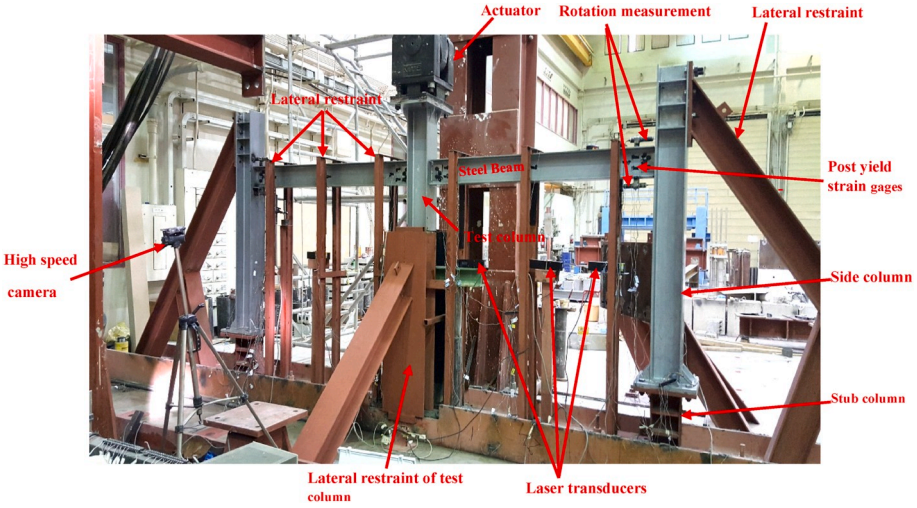

Fig. 3. Instrumented specimen ready for testing.

Table 3
Comparison of experimental and FE results[a].

Specimen ID	Results	Flexural action stage				Catenary action stage				P_u (kN)	Δ_u (mm)	E_u (kN.m	θ (degree)	Mode of failure
		P_y (kN)	Δ_y (mm)	$P_{u,FA}$ (kN)	$\Delta_{u,c\text{-}FA}$ (mm)	$P_{u,CA}$ (kN)	$P_{u,CA}/P_{u,FA}$	$\Delta_{u,c\text{-}CA}$ (mm)	$N_{u,CA}$ (kN)					
S-C	EXP	–	–	9	92	72.6	8.07	375	172	72.6	386	12.5	11.9	Fracture of tab plate
	FE	–	–	9	92	71.5	7.94	383	172	71.5	383	12.7	11.8	
	EXP/FE	–	–	1.00	1.00	1.02	1.02	0.98	1.00	1.02	1.01	0.98	1.01	
WUF-FW	EXP	198	25	257	97	316	1.23	213	79	316	213	72.5	6.0	Fracture of fillet weld
	FE	198	25	255	97	317	1.24	215	84	317	215	72.0	6.0	
	EXP/FE	1.00	1.00	1.01	1.00	1.00	0.99	0.99	0.94	1.00	0.99	1.01	1.00	
4 E-BUEEP-P	EXP	138	20	225	100	242	1.08	146	383	242	187	78.0	3.9	Fracture of end plate
	FE	138	20	223	100	240	1.08	139	373	240	173	73.5	3.7	
	EXP/FE	1.00	1.00	1.01	1.00	1.01	1.00	1.05	1.03	1.01	1.08	1.06	1.05	
CWP	EXP	147	35	201	115	603	3.00	518	1230	603	518	177.7	11.05	Fracture of top cover plate
	FE	166	34	199	115	590	2.97	540	1212	590	540	174.5	10.2	
	EXP/FE	0.89	1.03	1.01	1.00	1.02	1.01	0.96	1.02	1.02	0.96	1.02	1.08	
EPH	EXP	147	37	212	110	477	2.25	440	1035	477	476	120.6	7.5	Fracture of bolts
	FE	149	32	209	102	460	2.20	448	1014	460	453	118.3	7.3	
	EXP/FE	0.99	1.16	1.01	1.08	1.04	1.02	0.98	1.02	1.04	1.05	1.02	1.03	

[a] P_y = load at first yield of beam bottom flange at inner column face; Δ_y = displacement of middle column at first yield of beam bottom flange at inner column face; $P_{u,FA}$ = peak load of flexural action stage; $\Delta_{u,c\text{-}FA}$ = displacement of middle column at peak load of flexural action stage; $P_{u,CA}$ = peak load of catenary action stage; $\Delta_{u,c\text{-}CA}$ = displacement of middle column at peak load of catenary action stage; $N_{u,CA}$ = peak beam axial force at catenary action stage; P_u = progressive collapse resistance; Δ_u = displacement of middle column at ultimate state; E_u = energy dissipated at ultimate state; and θ = beam rotation at maximum load.

Stability can play a crucial role in the appearance and subsequent evolution of progressive collapse; mainly because the loading scheme includes gravitational loads. Stability manifests itself through a wide spectrum of different ways and therefore extreme caution should be exercised in order not to have possible instabilities and their effect on different types of connections. Instabilities may appear at the member level (column buckling), at the system level (global buckling), and at the local level (local instability - flange buckling). Several studies have been carried out to demonstrate how buckling/instability can be dominating in progressive collapse.

Gerasimidis [41] and Pantidis and Gerasimidis [42] presented a novel analytical framework for robustness assessment of two-dimensional (2D) steel gravity framed buildings under column-removal scenarios. The results revealed that the collapse of steel buildings is caused by different mechanisms for column removal from different stories. For example, when column removal occurs at lower floors, the collapse mechanism is governed by failure (buckling) of a column element. However, when column removal occurs at higher floors, the collapse mechanism is governed by flexural failure of the beams above the removed column, which is related to behavior of beam-column connections.

In recent papers [43,44], the importance of stability considerations under material and geometric nonlinearity analysis configuration is highlighted, in order to correctly identify the collapse modes and the corresponding collapse loads. The most common collapse modes included firstly yielding-type failure of beam elements above the removed column initiated by extensive plasticization, and secondly buckling of column elements adjacent to the removed column. Other modes of collapse also included shear failure of beam-column connections [45], or even loss of stability failure, which appears more often in tall and slender structures.

Recently, Kong et al. [46] carried out experimental study on progressive collapse potential of 3D steel frames under concentrated and uniformly distributed loading conditions. The authors found that the progressive collapse resistance decreases with the increase of vertical displacement and disappears when the vertical displacement is double the beam depth. The significant drop in progressive collapse resistance was attributed to different reasons. The most important of them was local buckling in compression zone of the steel beam, and this demonstrates the effect of local buckling on progressive collapse of flush end-plate connections.

In this study, three steel beam-column connections of different types were experimentally studied for progressive collapse risk of 2D assemblies under middle column loss scenario. Test frames comprised of three columns and two beams. These assemblies included one shear-connection specimen that signified the prevalent type of beam-column joint, and two IMF connection specimens designed and detailed as per ANSI/AISC 358–16 [37]. The IMF connection specimens involved: one welded unreinforced flange-fillet welded web and one bolted unstiffened extended end-plate with pretensioned high-strength bolts. The progressive collapse due to column-loss scenario was simulated by testing the steel frames after removing middle column and applying vertical downward load at a rate of 100 mm/s 3D finite element (FE) models were then prepared for the three specimens using ABAQUS software [47] taking into account nonlinear rate dependent material behavior and interfacial contact between different steel parts. The two steel IMF test assembly of Dinu et al. [36] were also utilized for validating the FE model parameters. The calibrated FE models were then extended to compare between the progressive collapse behavior of different types of steel IMF connections. These connections were designed and detailed as per ANSI/AISC 358–16 [37]; EN 1993-Eurocode 3 [38] or Turkish Earthquake Code TEC-2007 [39]. Performance of different IMF connections was compared based on their modes of failure and load-displacement response in both flexural and catenary action stages.

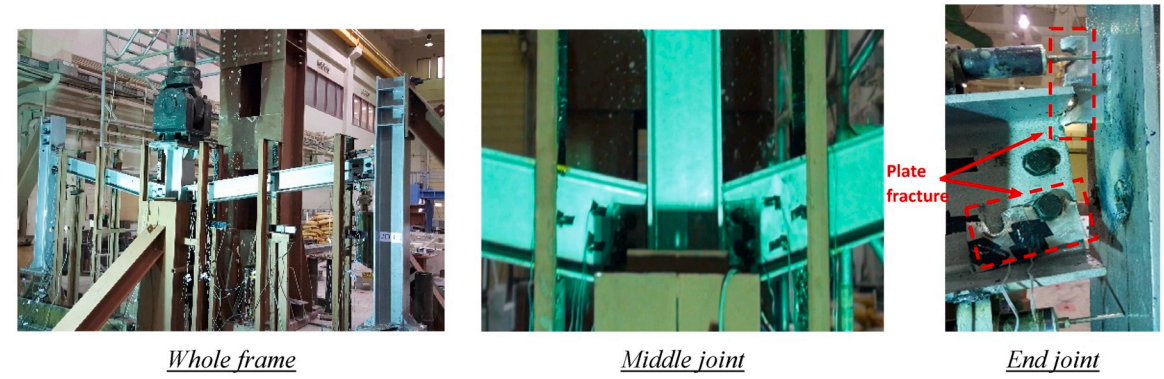

(a)

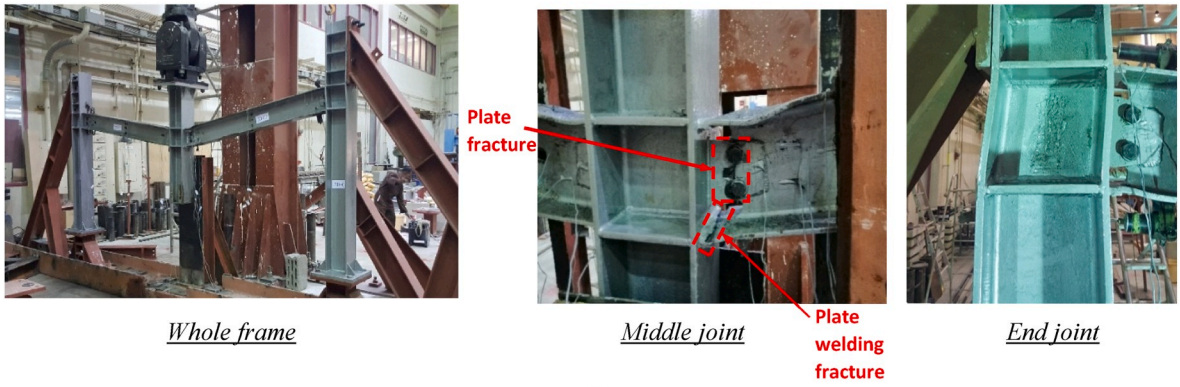

(b)

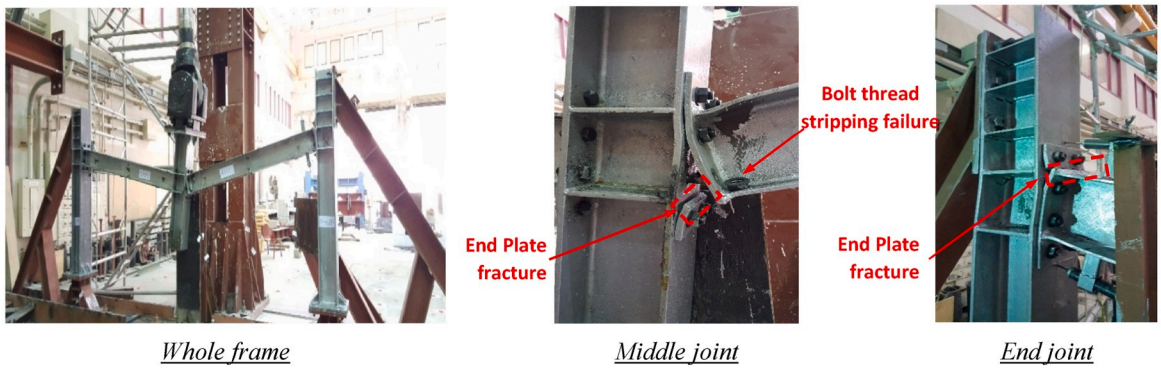

(c)

Fig. 4. Observed mode of failure for specimens tested in current study: (a) Specimen *S*–C; (b) Specimen WUF-FW; (c) Specimen 4 E-BUEEP-P.

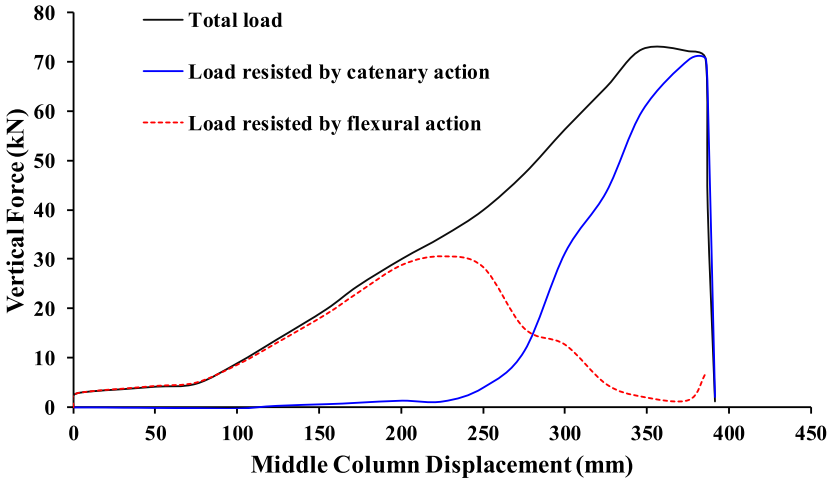

(a)

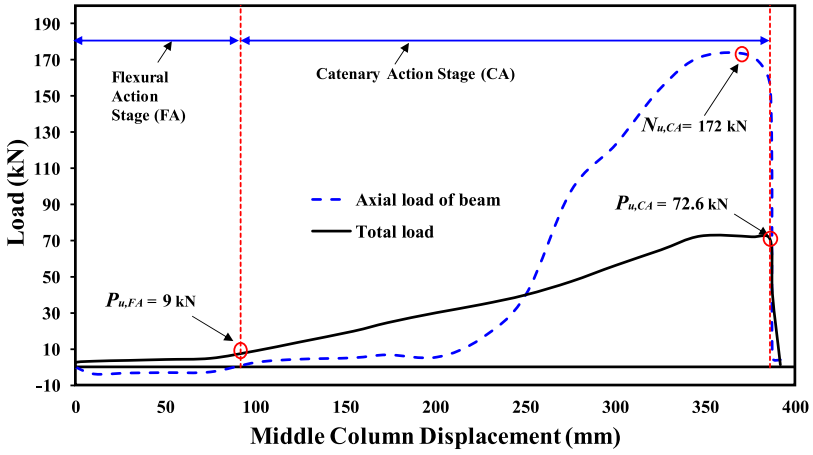

(b)

Fig. 5. Experimental load-displacement response for specimen *S*–C tested in current study: (a) Load-displacement curve; (b) Development of different action stages.

2. Experimental program

2.1. Details of test specimens

The goal of this research is to study the progressive collapse resistance of different steel beam-column joints in the event of missing a middle ground-story column of the exterior frame in an extreme event. To achieve this goal, a single story, two bay, prototype frame was selected. The two-bay prototype frame was assumed to be a part of an eight-story commercial steel building with four bays in each direction. The test specimens were designed to be one-third scale of the prototype perimeter frame. Three 2D steel frame assemblies having two bays, with details as shown in Table 1, were fabricated. Specimens were tested under vertical loading so as to obtain data for the severe damage in progressive collapse scenario. Fig. 1 shows these frame assemblies wherein the middle short column represents the test column for simulating the column loss scenario. Out of the three specimens, the first one (specimen *S*–C) was designed with shear-type beam-column connection and was used as a control specimen. The control test specimen represents one of the most prevalent steel beam-column joints in non-seismic regions. The second specimen (WUF-FW) was designed as an IMF beam-column connection, which is welded unreinforced flange-fillet welded web. The third test frame was also designed as an IMF beam-column connection that is bolted unstiffened extended end-plate with pretensioned high-strength bolts (4 E-BUEEP-P). All specimens have the span with center-to-center spacing of columns as 2 m and the total column height as 2 m (Fig. 1). Beam-column connection details for the three test specimens are depicted in Fig. 2. For all specimens, the rolled steel section H 194 × 150 was used in beams while the rolled steel section of H 200 × 200 was used for columns, as seen in Table 1 and Figs. 1 and 2.

Fig. 2(a) shows the connection used in the first specimen *S*–C, which was single-plate shear connection. The web of the beam was connected to the 6-mm shear plate with the help of two M16 high-strength bolts of grade 10.9. The shear plate was welded to the column flange using fillet welding. The design of the welded joint was as per the provisions of AISC [48]. Fig. 2(b) shows the second specimen WUF-FW, which was fabricated using IMF connection. The fillet welding was used to connect the beam flanges with the column flange, while the web of the beam was connected to a shear plate (pre-welded to the beam web and column flange) using two M16 high-strength bolts of grade 10.9. The design of the connection was as per the ANSI/AISC 358–16 provisions [37] but the difference was in the method of welding, whereas fillet welding was utilized instead of complete joint penetration welding (CJP). The connection used in the third specimen 4 E-BUEEP-P was also IMF connection, as shown in Fig. 2(c). The end-plate bolted connection was prepared by welding an end-plate to the beam and bolting the column

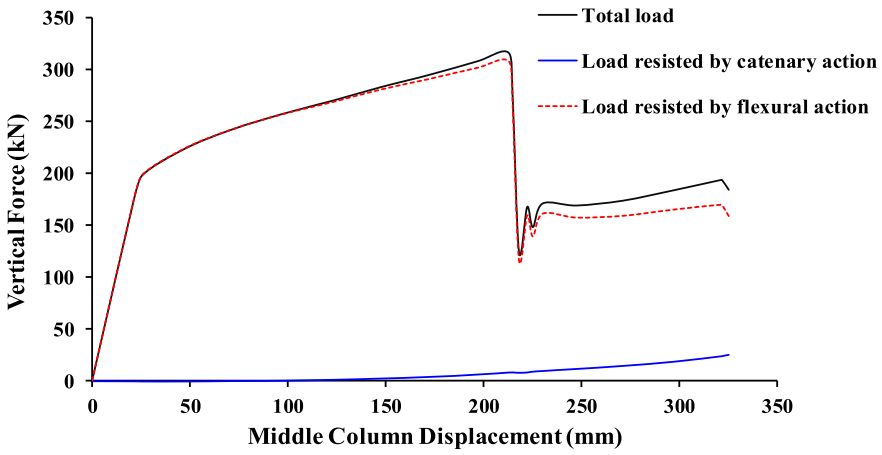

(a)

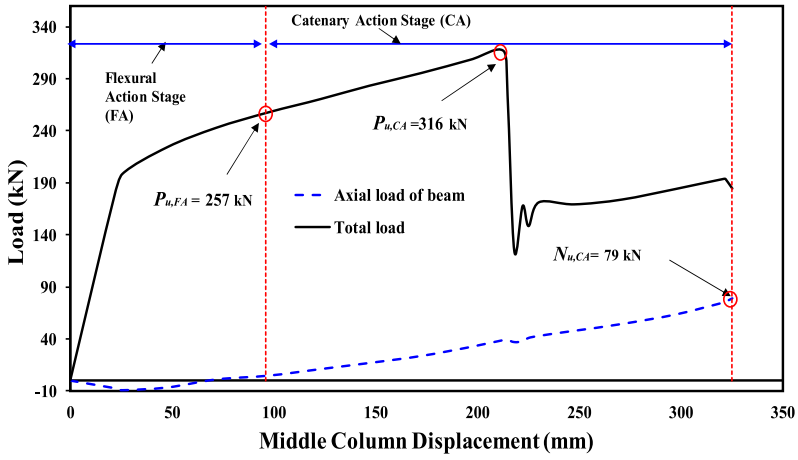

(b)

Fig. 6. Experimental load-displacement response for specimen WUF-FW tested in current study: (a) Load-displacement curve; (b) Development of different action stages.

flange to the end-plate using pretensioned high-strength bolts (M20–10.9). All bolts were subjected to direct tension force of 179 kN, as specified in the ASTM A490M-14a [49]. The design of the connection was as per the ANSI/AISC 358–16 provisions [37]. Before testing of frame assemblies, coupons prepared from the columns, beams, and plates were tested, for establishing the mechanical properties of the steel used in these members. The bolts were also tested to assess their mechanical properties. Measured material properties of different components of test specimens are summarized in Table 2. In addition to the three specimens tested in this study, another two IMF connection specimens (CWP and EPH) that were tested in literature by Dinu et al. [36] (see Fig. 2(d) and (e) and Table 1) was used for validating the FE modeling.

2.2. Test setup and instrumentation

In order to simulate the boundary conditions of the prototype building during the testing, it was necessary to restrain the lateral out-of-plane movement possibility at the level of the beams (see Figs. 1 and 3). Moreover, the two outer columns of the test assembly were partially extended above the beam level with the top ends restrained with stiff bracing, as presented in Figs. 1 and 3. These bracings were stiff in order to represent the continuity of beams and columns in horizontal and vertical directions, respectively. This simulation may be valid due to the structural layout of the prototype building as two other exterior columns exist to the left (or right) of the removed column. Also, seven full stories lie above the studied ground-story columns. However, in case of less number of outer columns adjacent to the removed one and/or in the case of low rise buildings, provision of stiff bracing at the top ends of outer columns of the test assembly may not be realistic and softer bracing may be used instead. In conclusion, the bracing system provided in this study is provisional and should be only used in case of missing interior column scenarios in multi-story (medium to high rise buildings), multi-bay frames (the removed column should have at least two adjacent exterior columns in either direction). It should be also noted that the bracing system used in this research is similar to other studies available in the literature [30,34,36,50].

The exposure of a building to blast loading may lead to the sudden removal of a column, which may lead to the progressive collapse of the structure. In real progressive collapse scenarios due to blast threats, the column is removed suddenly with high speed. This sudden column loss scenario was simulated in our experiments by releasing the support of the middle test column and applying sudden load on that column using a 1000-kN fatigue-rated MTS actuator at a rate of 100 mm/s. However, the high speed in real progressive collapse events cannot be accommodated in the experiments due to the limits of the used actuator. The

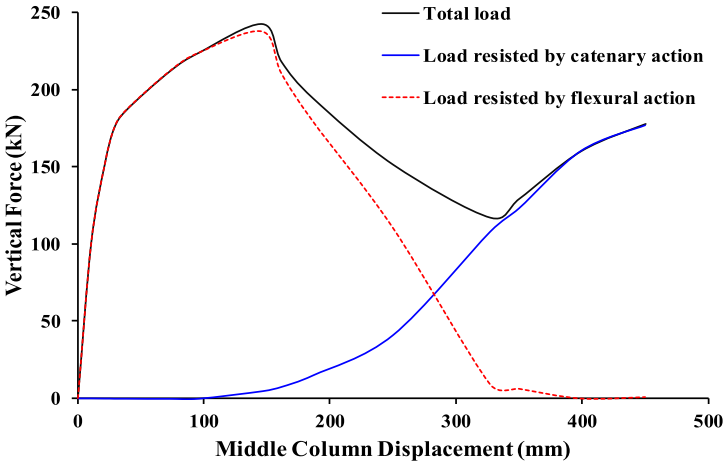

(a)

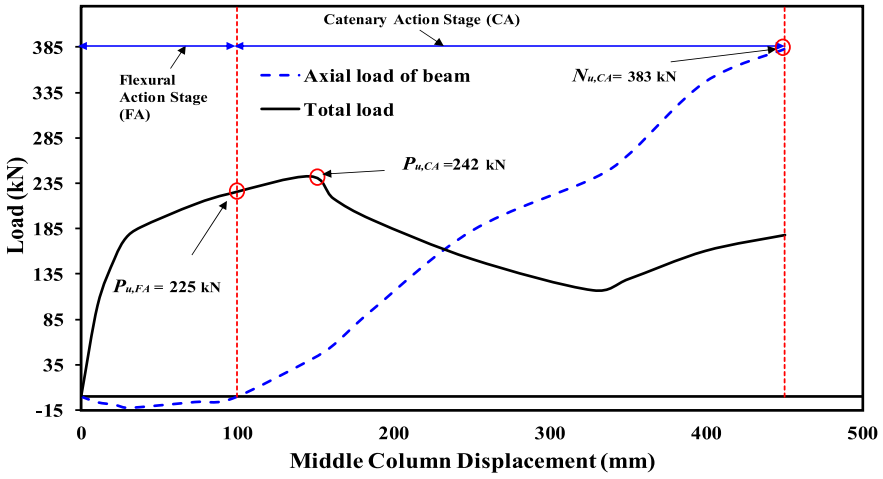

(b)

Fig. 7. Experimental load-displacement response for specimen 4 E-BUEEP-P tested in current study: (a) Load-displacement curve; (b) Development of different action stages.

loading rate adopted (i.e. 100 mm/s) was similar to quasi-static type testing. Thus, the inertial effects in experiments were of smaller scale than expected in a column-removal scenario. However, the increase in stresses due to the inertial forces is partly compensated by the enhanced material strength due to strain rate effect. It is also worth mentioning here that the loading protocol used in the tests of this study was used in many other similar tests conducted by the authors [51–53].

Instrumentation was done for measuring displacements, joint rotation, and strains in the critical regions of the test frame. The laser transducers, located at different sections of the beam (Fig. 3), were used for the precise measurement of beam displacements. The middle column was subjected to displacement controlled downward load with the help of the actuator in steps of incremental vertical displacement up to failure. Post-yield strain gages were affixed at critical areas of beam-column joints to monitor the beam strains as seen in Fig. 3. Pretest simulations using ABAQUS [47] software were performed to roughly estimate the response of the test frame.

3. Test results and discussion

The experimental results for the three tested specimens of this study are summarized in Table 3. The test results of specimens CWP and EPH tested by Dinu et al. [36] are also reported in this table. Test results include key elements of load-displacement curve such as: (i) load at first yield of the beam bottom flange on inner face of the column, (ii) peak loads corresponding to the flexural and catenary action stages, (iii) middle column displacement at first yield of the bottom flange of beam at inner joint, (iv) middle column displacements at peak loads corresponding to the flexural and catenary action stages, (v) middle column displacement at ultimate, (vi) peak axial force in beam corresponding to the catenary action stage, (vii) energy dissipated at ultimate state, (viii) beam rotation at maximum load, and (ix) mode of failure. It is worth stating that the ultimate condition is taken as that where the load in post-peak stage decreases by 20% of its maximum value [54].

To compute axial force in the beams $N_{u,CA}$, the axial strain variation in beam section along the beam depth was measured using strain gages as seen in Fig. 1(b). Strains were then used to compute distribution of normal stresses, which were integrated to calculate the beam axial force. The rotations at the beam ends (θ) are taken as same. The total resistance P_u of an assembly consists of two components: resistance due to flexural action ($P_{u,FA}$) and resistance offered by the catenary action ($P_{u,CA}$). These components can be approximately calculated from

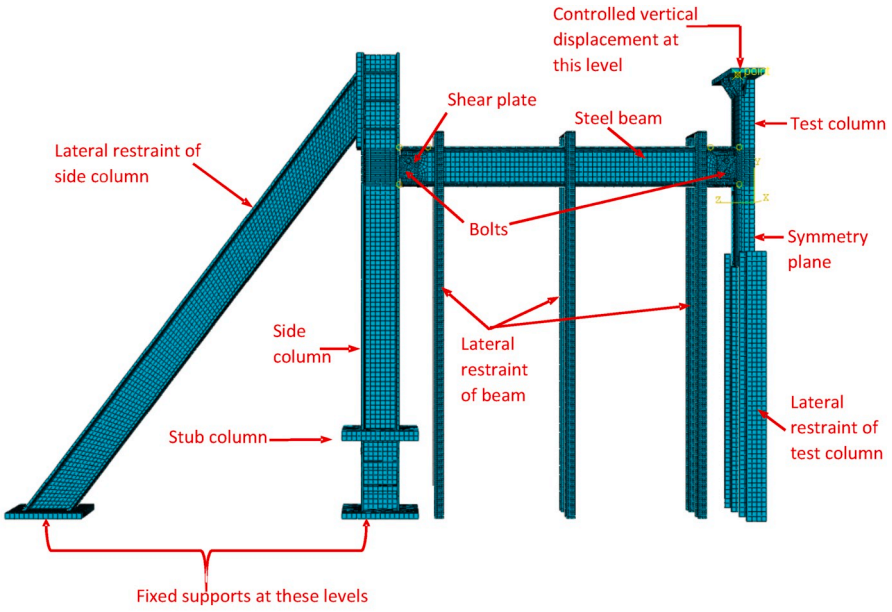

(a)

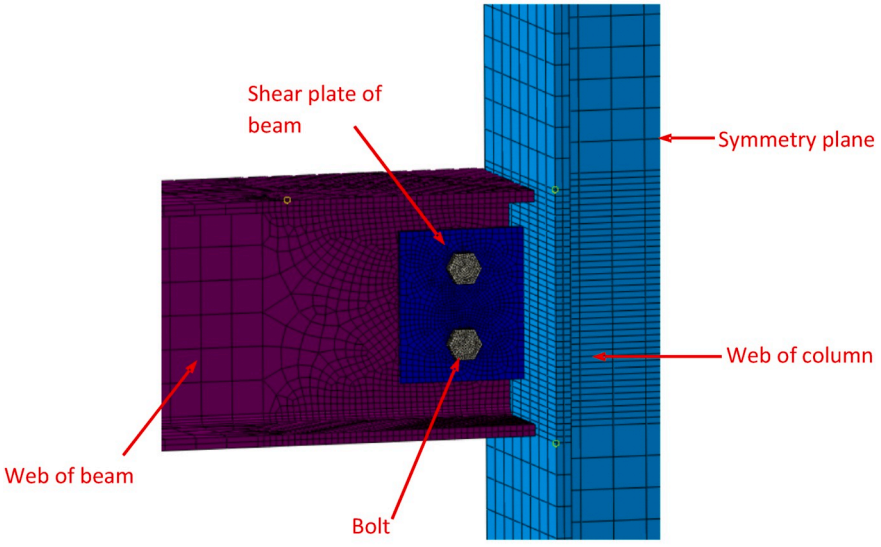

(b)

Fig. 8. FE model for *S*–C specimen: (a) General view of FE model; (b) Detailed view of middle beam-column joint.

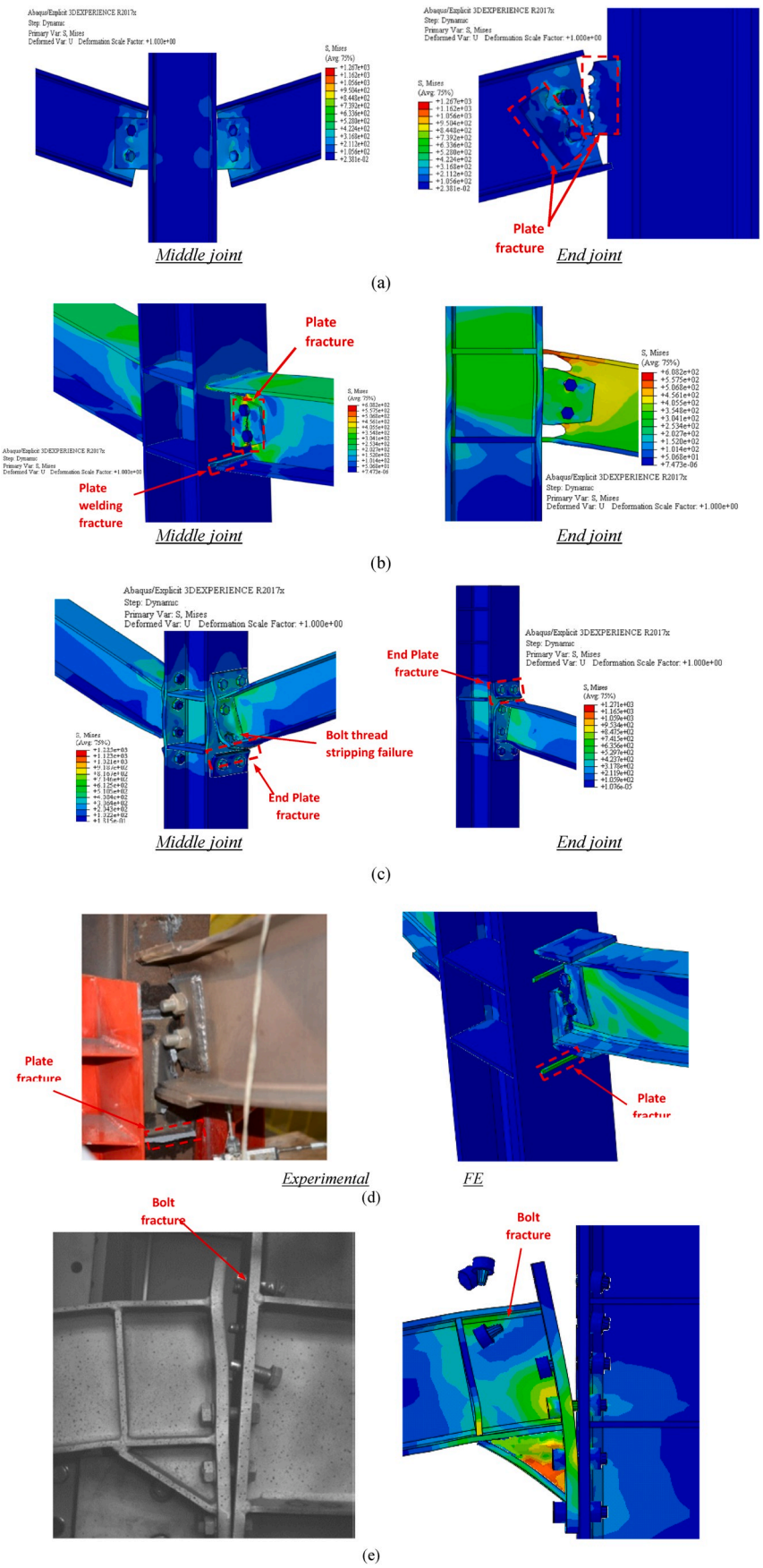

Fig. 9. FE mode of failure for: (a) Specimen *S*–C of current study; (b) Specimen WUF-FW of current study; (c) Specimen 4 E-BUEEP-P of current study; (d) Specimen CWP tested by Dinu et al. [36]; (e) Specimen EPH tested by Dinu et al. [36].

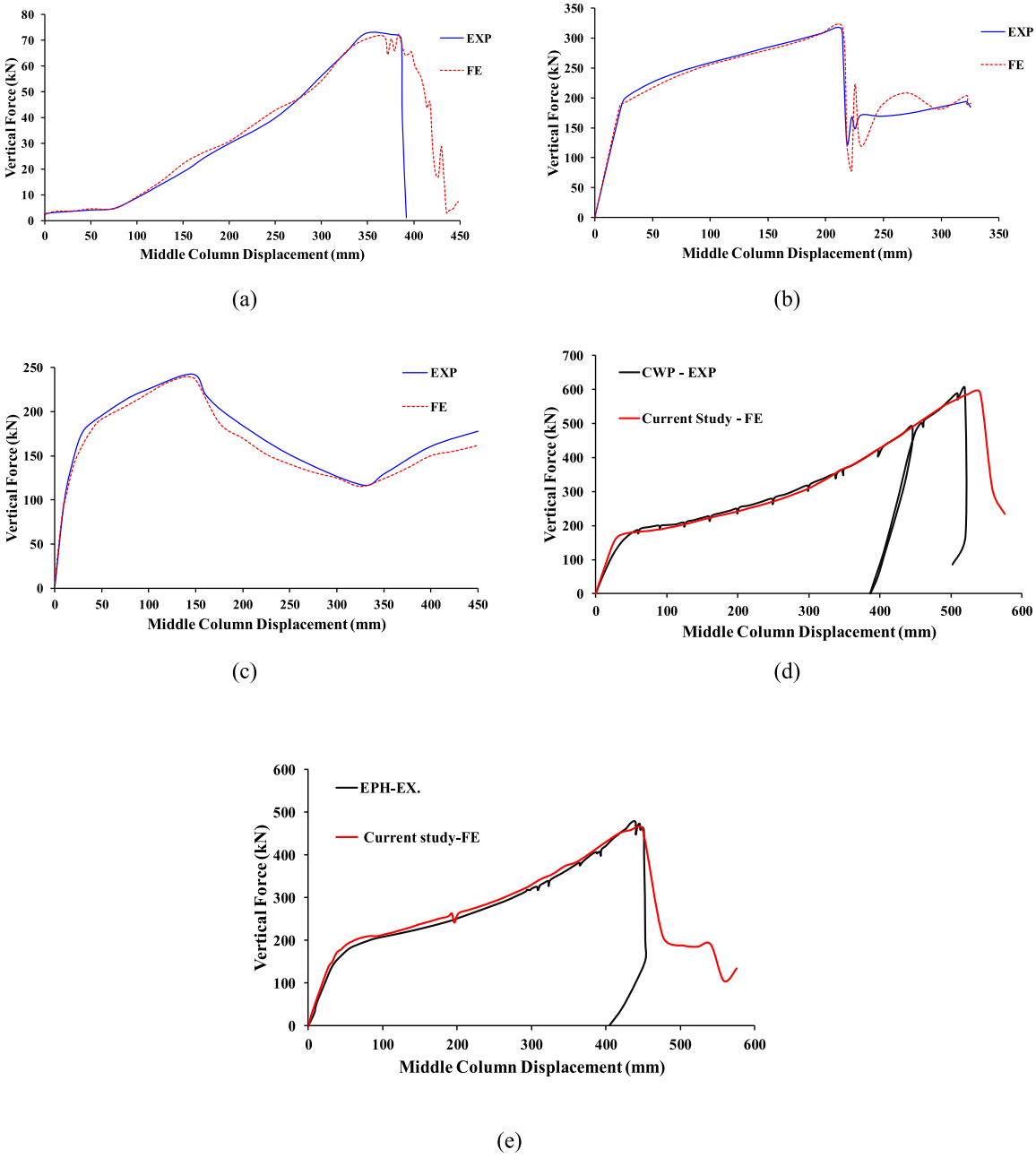

Fig. 10. Comparison of experimental and FE load-displacement curves for: (a) Specimen *S*–C of current study; (b) Specimen WUF-FW of current study; (c) Specimen 4 E-BUEEP-P of current study; (d) Specimen CWP tested by Dinu et al. [36]; (e) Specimen EPH tested by Dinu et al. [36].

$$P_{u,CA} = 2\ N_{u,CA} \sin\theta \quad (1)$$

$$P_{u,FA} = P_u - P_{u,CA} \quad (2)$$

Eqs. (1) and (2) were used to compute the peak vertical loads at flexural and catenary action stages, respectively, enlisted in Table 3 for the test specimens. Test results for each specimen are briefly discussed below.

3.1. Simple connection (S–C)

Observed failure mode of control specimen *S*–C is presented in Fig. 4 (a). It is revealed that the loss of column under an extreme load case in steel buildings with shear connection makes them susceptible to progressive collapse. The rotation of specimen at the two ends with the increase in the mid-span deflection is a typical characteristic of such simple connections with limited moment resisting capacity. Fig. 5 displays the load-displacement characteristics for specimen *S*–C. Up to displacement of 75 mm, the specimen could resist small loading as seen in Fig. 5. Tensile beam axial force was mobilized at a displacement of 92 mm, which indicates the initiation of catenary behavior stage (Fig. 5(b)). Further increase in load caused bearing deformations of bolt holes in the shear plate. When the load level reached 72.6 kN, complete fracture of the shear tabs at right connection occurred leading to the total collapse of the frame (Figs. 4(a) and 5). The displacement of middle column recorded at this stage was 386 mm ($\theta = 11.9°$).

3.2. Moment connection (WUF-FW)

As mentioned previously, fillet welding was utilized for moment

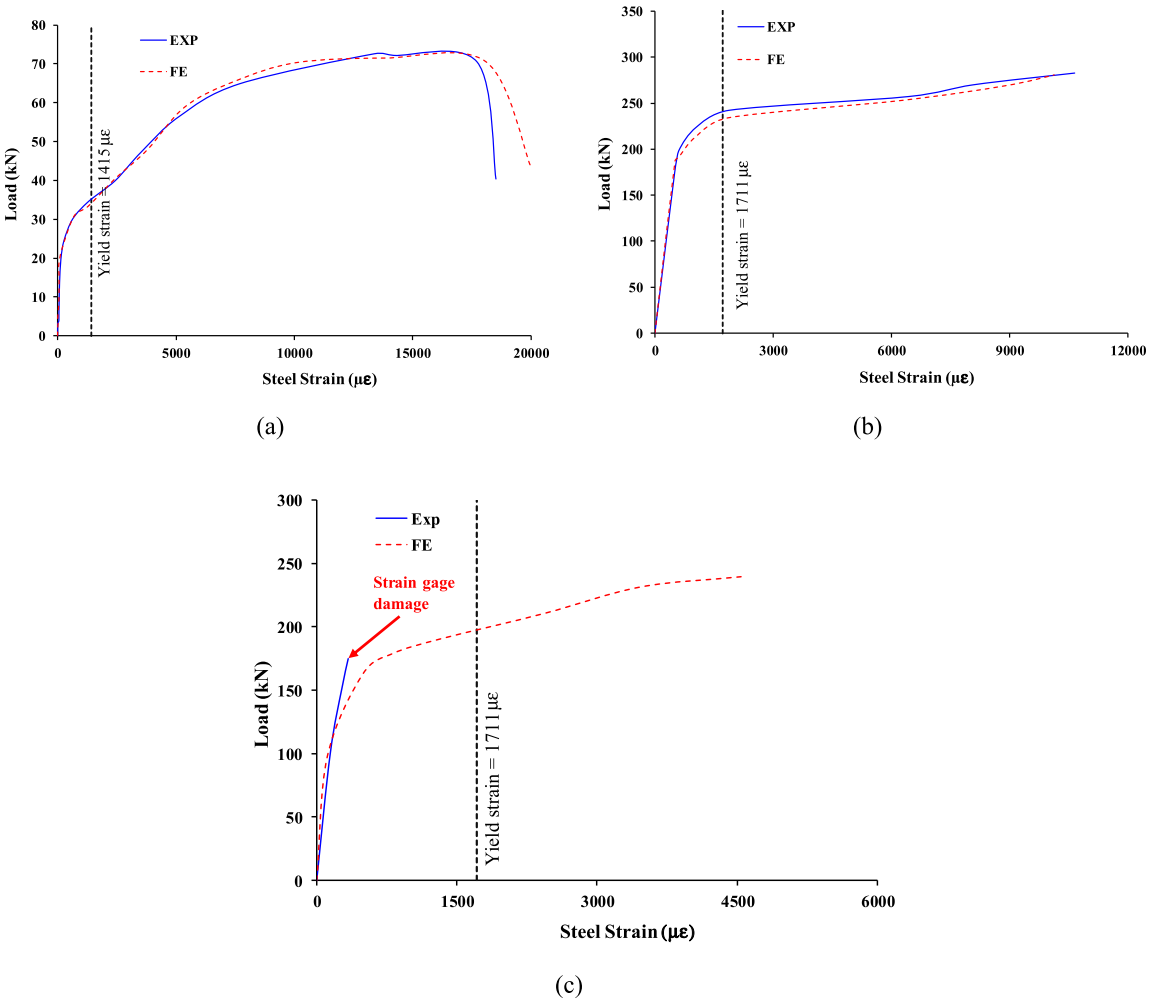

Fig. 11. Comparison of experimental and FE load vs strain plots for: (a) Shear plate strain at middle joint for specimen *S*–C; (b) Beam bottom flange strain at face of inner joint for specimen WUF-FW; (c) Beam bottom flange strain at face of end plate of middle joint for specimen 4 E-BUEEP-P.

Table 4
Details of FE matrix for different types of IMF connections.

Specimen ID	Bolt	Beam-column connection details
Connections designed as per ANSI/AISC 358–16 [37]		
WUF-W	Bearing	Same as WUF-FW (using CJP welding) (see Fig. 12 (a))
RBS	Bearing	Same as WUF-W specimen but with reduced beam section (see Fig. 12(b))
4 E-BUEEP	Bearing	Same as 4 E-BUEEP-P specimen but with pretensioned bolts (see Fig. 12(c))
4 E-BSEEP	Bearing	Bolted stiffened extended end plate (see Fig. 12(d))
4 E-BSEEP-P	Pretensioned	Same as 4 E-BSEEP specimen but with pretensioned bolts (see Fig. 12(d))
BFP	Bearing	Same as *S*–C specimen but with bolted flange plate (see Fig. 12(e))
KBB-W	Bearing	Same as *S*–C specimen but with welded flange bracket (see Fig. 12(f))
KBB-W-P	Pretensioned	Same as KBB-W specimen but with pretensioned bolts (see Fig. 12(f))
Connections designed as per EN 1993- Eurocode 3 [38]		
BHJ	Bearing	Bolted hunched joint (see Fig. 12(g))
BHJ-P	Pretensioned	Same as BHJ specimen but with pretensioned bolts (see Fig. 12(g))
Connection designed as per TEC-2007 [39]		
WJFP	Bearing	Same as *S*–C specimen but with welded flange plate (see Fig. 12(h))

connection WUF-FW between beam and column flanges due to its local availability and constructability. Even though this connection did not fully as per the provisions of ANSI/AISC 358–16 [37], its performance was much better than the simple shear-connection specimen *S*–C in terms of flexural stiffness and progressive collapse resistance as seen in Fig. 6. Also, as depicted from Table 3, the rotation of *S*–C connection under column-loss scenario is about twice as large as rotation of WUF-FW connection. From Fig. 6, it is clear that initially up to a load level of 197 kN and corresponding deflection of 25 mm, the WUF-FW specimen exhibited elastic state as the load increased linearly with the increase in displacement. Subsequently the flexural stiffness started to decrease. The fracture in the welding between bottom flange of right beam and middle column was observed at 210 mm displacement (Fig. 4 (b)). This caused the load to drop suddenly from 316 kN (peak load) to 130 kN, as shown in Fig. 6(a). After that, the specimen failed completely due to fracture of the shear tabs at right beam, as shown in Fig. 4(b). It is noted that the WUF-FW connection could sustain substantial flexural action at the full displacement range. In fact, at large displacement levels, the catenary action stage was not fully mobilized and the axial beam forces were considerably small with peak value of 79 kN as seen in Fig. 6(b).

3.3. Moment connection (4E-BUEEP-P)

For moment connection 4 E-BUEEP-P, the test frame went through three stages. The specimen was initially stiff, as the bolts were

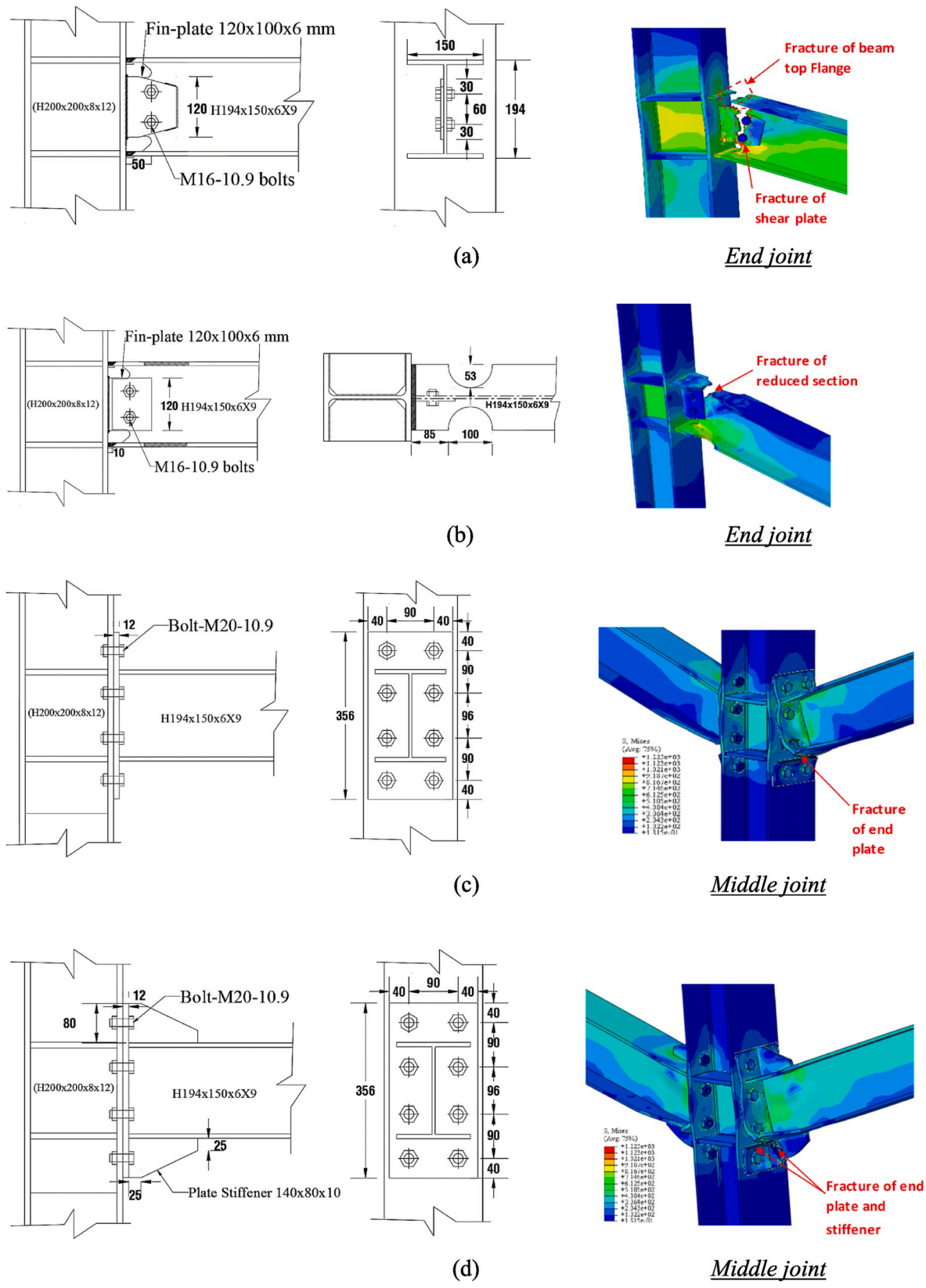

Fig. 12. Details and FE mode of failure for different types of IMF connection specimens (Note: All dimensions are in mm): (a) Specimen WUF-W; (b) Specimen RBS; (c) Specimen 4 E-BUEEP; (d) Specimens 4 E-BSEEP & 4 E-BSEEP-P; (e) Specimen BFP; (f) Specimens KBB-W & KBB-W-P; (g) Specimens BHJ & BHJ-P; (h) Specimen WJFP.

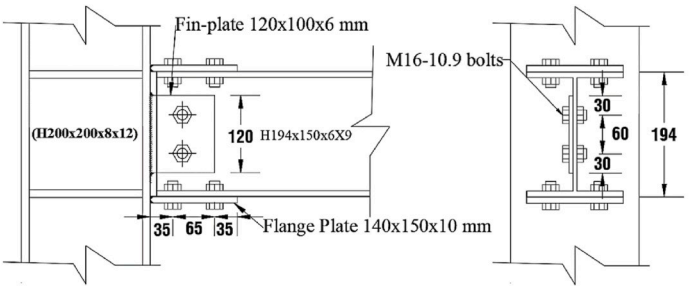

(e)

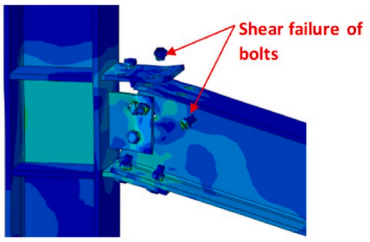

End joint

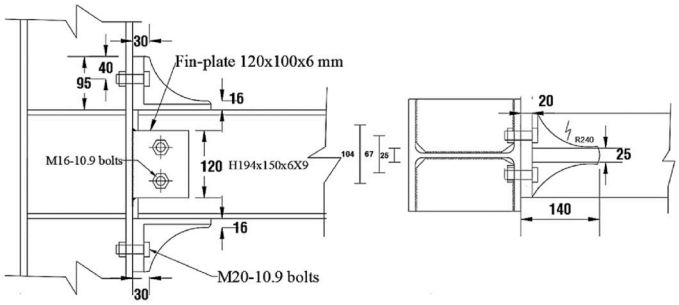

(f)

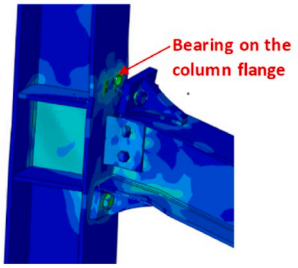

End joint

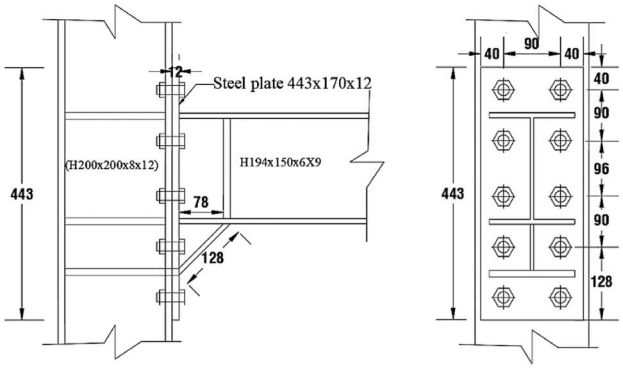

(g)

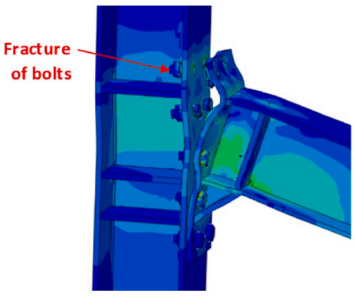

End joint

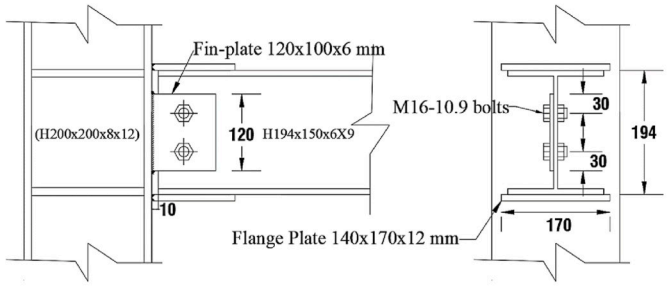

(h)

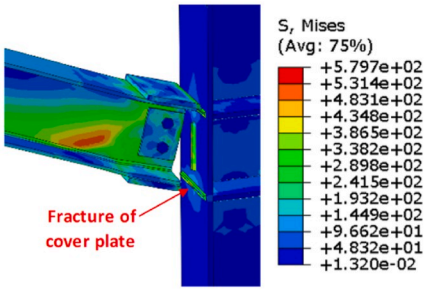

Middle joint

Fig. 12. (*continued*).

Table 5
Summary of FE results for all IMFs connections[a].

Specimen ID	Flexural action stage				Catenary action stage				P_u (kN)	Δ_u (mm)	E_u (kN. m	θ (degree)	Mode of failure
	P_y (kN)	Δ_y (mm)	$P_{u,FA}$ (kN)	$\Delta_{u,c\text{-}FA}$ (mm)	$P_{u,CA}$ (kN)	$P_{u,CA}/P_{u,FA}$	$\Delta_{u,c\text{-}CA}$ (mm)	$N_{u,CA}$ (kN)					
Designed and detailed in accordance with ANSI/AISC 358–16 [37]													
WUF-W	190	25	256	98	577	2.3	385	1062	577	422	158.5	10.9	Fracture of beam flange
RBS	177	18	256	157	520	2.0	461	939	520	490	164.2	13.0	Fracture of beam flange at reduced section
4 E-BUEEP	118	19	220	139	240	1.1	139	373	240	178	72.5	3.9	Fracture of end plate
4 E-BSEEP	163	18	263	142	345	1.3	303	624	345	375	130.0	8.6	Fracture of end plate and stiffener
4 E-BSEEP-P	171	18	263	142	345	1.3	304	624	345	343	131.0	8.6	Fracture of end plate and stiffener
BFP	23	25	253	132	260	1.0	148	471	260	210	75.7	4.2	Shear failure of bolts
KBB-W	98	11	295	96	299	1.0	120	532	299	190	73.2	3.4	Bearing on column flange
KBB-W-P	104	11	295	96	299	1.0	120	532	299	190	73.6	3.4	Bearing on column flange
Designed and detailed in accordance with EN 1993- Eurocode 3 [38]													
BHJ	161	21	236	137	458	1.9	370	852	458	414	148.5	10.4	Fracture or thread stripping failure of bolts.
BHJ-P	170	21	236	137	458	1.9	370	852	458	370	149.3	10.4	Fracture or thread stripping failure of bolts.
Designed and detailed in accordance with TEC-2007 [39]													
WJFP	162	11	345	107	650	1.9	368	1178	650	383	179.4	10.4	Fracture of cover plate

[a] P_y = load at first yield of beam bottom flange at inner column face; Δ_y = displacement of middle column at first yield of beam bottom flange at inner column face; $P_{u,FA}$ = peak load of flexural action stage; $\Delta_{u,c\text{-}FA}$ = displacement of middle column at peak load of flexural action stage; $P_{u,CA}$ = peak load of catenary action stage; $\Delta_{u,c\text{-}CA}$ = displacement of middle column at peak load of catenary action stage; $N_{u,CA}$ = peak beam axial force at catenary action stage; P_u = progressive collapse resistance; Δ_u = displacement of middle column at ultimate state; E_u = energy dissipated at ultimate state; and θ = beam rotation at maximum load.

pretensioned, till a middle column displacement of 29 mm at which separation was initiated at the middle joint between the column flange the end plate. This corresponds to a load of 175 kN. Upon separation, there was reduction in flexural stiffness (Fig. 7) and the end plate in the right beam near the middle joint started to bend, as seen from Fig. 4(c). Fig. 7(b) shows that the beam axial force was almost negligible until the bending of the end plate. The fracture of end plate at the bottom of the right hand beam near the middle column occurred at a displacement of 146 mm, which corresponds to the maximum applied load of 242 kN. Further increase in displacement to 175 mm caused thread stripping failure of the bolts in the bottom second row (see Fig. 4(c)) and this was the third stage. There was only a minor effect of the axial load, the fractures occurred mainly due the flexure. The end plates of the left and right joints also fractured at a displacement of 250 mm. Fig. 7(a) shows that further increase in displacement to approximately 350 mm leads to the increase in the load. The high magnitude of tension at this stage causes the fracture of bolts of 2nd row from the top of the left hand and right hand connections through the stripping of bolt thread.

4. Finite element modeling

The general purpose software ABAQUS [47] was employed in the FE modeling of test specimens. It should be noted that accounting for its symmetry, the FE model was prepared for only one-half specimen assembly. Below are the details of the FE models.

4.1. Mesh generation

Illustrated in Fig. 8(a) is the FE mesh for test frame *S*–C. In the generation of the FE mesh, 8-node reduced integration solid elements were utilized for different frame components (beams, columns, bolts and shear plates) [55]. The size of solid elements in the FE model ranged from 2 to 25 mm. A dense fine mesh was used for bolts (2.0 mm) while for the other components (shear plates, columns and beams), size of elements was nearly 5 mm at the ends of beam, where shear plates fractured (Fig. 8(b)).

4.2. Material modeling

The material model is based on tensile testing of standard steel coupons which were prepared and then tested as per relevant standards [56] (see Table 2). The engineering stress-strain (σ_E - ε_E) curve extracted from the test was transformed into a true stress versus true strain (σ_{true} - ε_{true}) curve up to the ultimate force with the following equations [38]:

$$\sigma_{true} = \sigma_E(1 + \varepsilon_E) \tag{3}$$

$$\varepsilon_{true} = \mathrm{In}(1 + \varepsilon_E) \tag{4}$$

After the maximum load is reached, due to necking, the material seems to soften, while it is actually hardening [57,58]. The material curve for true stress-true strain beyond the maximum load of the engineering stress-strain curve was considered ascending with a parabolic shape. It is worth mentioning that the input parameters for the parabolic curve are not the same for all model components and they were obtained from coupon tests conducted on different parts (e.g. beam flange, beam web, column flange, column web, and tab plates). This shape was obtained through iterations by calibrating the FE model results with coupon test results. Fracture of steel observed in the experiments was modeled using element deletion following the principle of "damage for ductile metal" available in software [47]. Strain rate effects were incorporated in the material model. It is worth noting that the damage parameters used in the material model are directly related to the size and shape of the FE mesh [55].

The general contact type was defined between elements of bolts, webs, and shear tabs. Coefficient of friction of 0.3 was assumed between steel elements which are initially in contact [47,52]. For pre-tensioned moment connection 4 E-BUEEP-P, pressure was applied to the two bolt surfaces to model the pre-tensioning force. The welds between different steel components were simulated by "tie" contact interface.

4.3. Loading and boundary conditions

The boundary conditions used in the FE model simulated precisely the boundary conditions of the test frames (see Fig. 8). Lateral beam and column supports were provided in the FE model at locations similar to the experiment as seen in Fig. 8. It should be noted that the out-of-plane

displacement of the beam flanges were restrained at locations where lateral supports are provided. The fixed column base was simulated by restraining both displacement and rotation at bottom nodes in the global X, Y and Z directions (see Fig. 8).

The FE simulation was carried out using the explicit module of ABAQUS software, which has been validated earlier for modeling of the progressive collapse of building structures [35,36,55,59]. Accounting for symmetry in the test frames, only one-half of the specimen was simulated as shown in Fig. 8(a). Symmetry boundary conditions were assigned to the nodes lying on the symmetry plane. Displacement-time history was assigned to the top nodes of the test column to simulate the displacement-controlled loading used in the tests, where vertical displacement increased at a rate of 100 mm/s to simulate the experiments.

4.4. FE model validation

The experimental results of the three specimens tested in this study in addition to two specimens CWP and EPH tested by Dinu et al. [36] were used for validating the FE models. The FE analysis results are discussed in term of load-displacement response and mode of failure.

Comparison between observed and numerically predicted key load-displacement results for the 5 test frames is shown in Table 3. Compared with test results, deviations of 0%–1% and 0%–4% were, respectively, predicted for peak load of flexural and catenary action stages. Deviations of 0%–8% and 1%–5% were also predicted for center column displacement at peak load of flexural and catenary action stages, respectively. Nevertheless, compared with the test results, deviation of 0%–6% was noticed for peak beam axial force at catenary action stage. It is also explicable from Table 3 that the energy dissipation at ultimate state (area under load versus displacement curve) was efficiently predicted by the numerical modeling with errors in prediction varying from 1% to 6%.

Presented in Fig. 9 are the numerically predicted failure modes of the 5 test frames and it is noticed that they agree well with the experiments. Depicted in Fig. 10(a) to 10(d) are comparisons between measured and predicted load versus center column displacement envelopes for the 4 test frames and good match was found between the experimental and numerically predicted curves, especially for the ultimate load. Additionally, as depicted from Fig. 10(a) to 10(d), the stiffness of the test

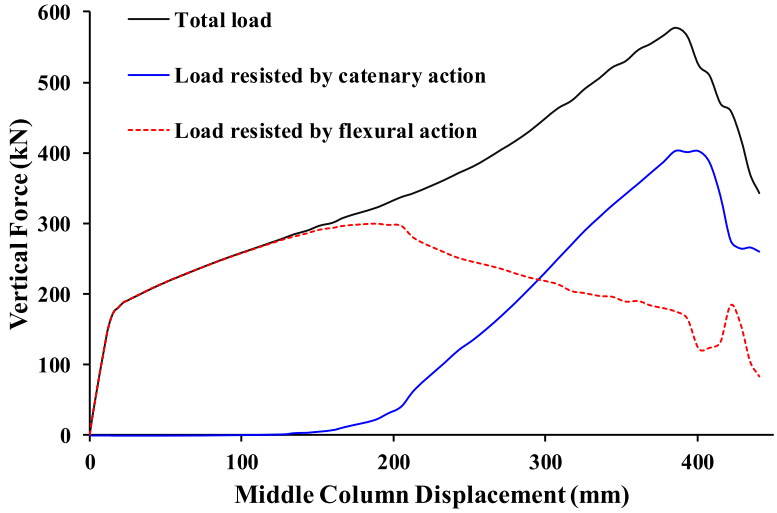

(a)

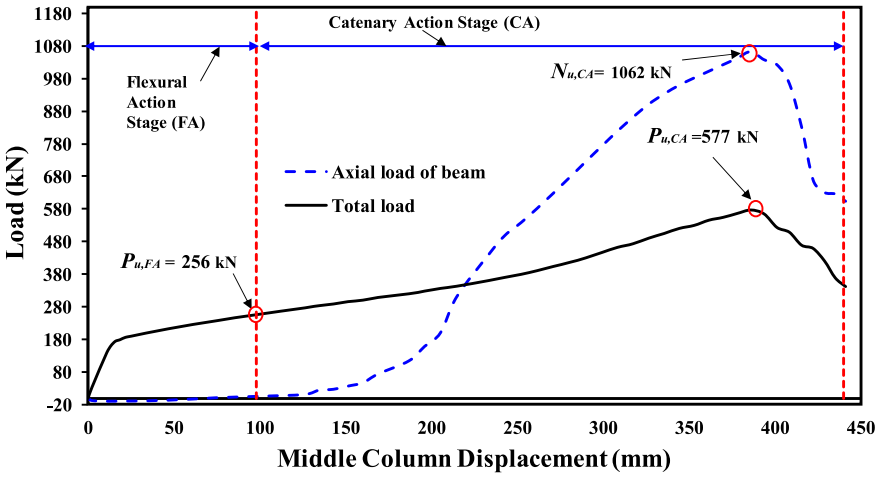

(b)

Fig. 13. FE load-displacement response for specimen WUF-W: (a) Load-displacement curve; (b) Development of different action stages.

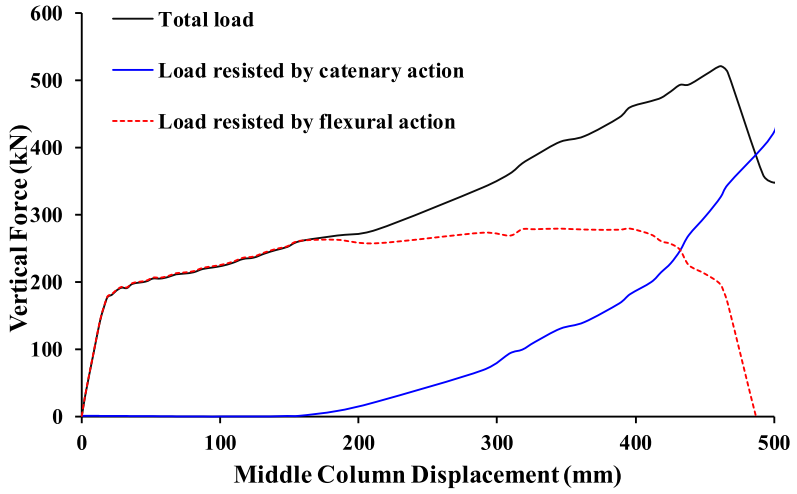

(a)

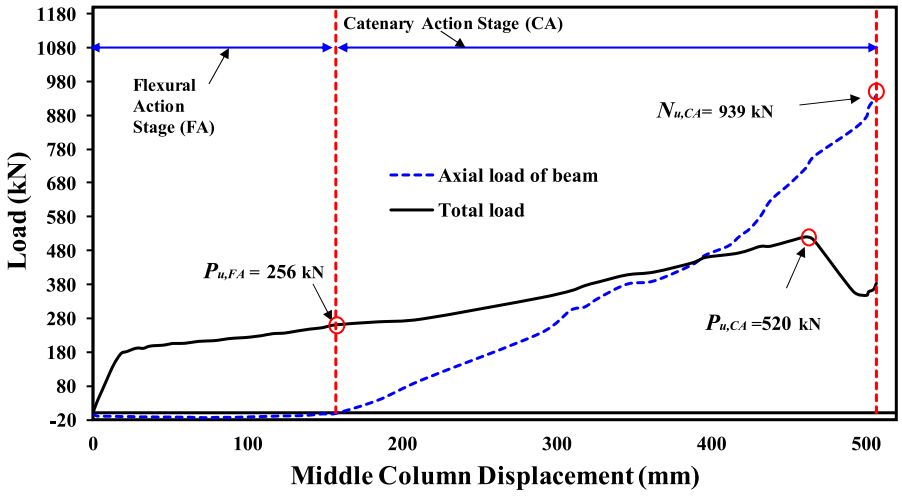

(b)

Fig. 14. FE load-displacement response for specimen RBS: (a) Load-displacement curve; (b) Development of different action stages.

frames at all range of response was well numerically assessed in comparison with the tests. The descending portion of the load-displacement response was also well predicted by the FE models (Fig. 10(a) to 10(d)), which reveals the precision of the constitutive modeling.

Additionally, predicted load versus steel strain plots are compared with the measured ones as depicted in Fig. 11 for the three specimens tested in current study. For the specimens tested by Dinu et al. [36], measured strain plots were not available and hence the comparison graphs were not generated. For specimen *S*–C, Fig. 11(a) shows the comparison of measured and predicted load versus shear plate strain curves at the middle joint. As seen in the figure, good match was achieved till the peak load. For test specimen WUF-FW, Fig. 11(b) illustrates the comparison for load versus beam bottom flange strain curves at the face of the inner joint. Good agreement was also obtained between the experimental and numerically predicted curves. For specimen 4 E-BUEE-P, Fig. 11(c) presents the comparison between observed and predicted load versus beam bottom flange strain curves at the face of end plate of the middle joint. Due to damage of the strain gage in the test, the experimental curve was stopped at a steel strain of about 550 με, and fairly good agreement between the two curves could be observed till this point.

The numerically developed models were thus calibrated for both simple shear and IMF connections and hence can be extended for studying the progressive collapse behavior of different types of steel IMF connections under column-loss scenarios as will be discussed in the next section.

5. Numerical investigation of different IMF connections

In this section, eleven types of IMF connections were numerically investigated under middle column-loss scenarios as displayed in Table 4. These included eight connections in accordance with ANSI/AISC 358–16 [37], two connections in conformance with EN 1993-Eurocode 3 [38], and one connection as per TEC-2007 [39]. Design and detailing of all connections were conducted to satisfy the seismic design criteria for steel intermediate moment frames. As illustrated in Table 4, out of the 11 specimens, three connections were designed with pretensioned bolts. It should be noted that the designation used in this study for connections (given in Table 4) is the same as that used in codes and standards. Fig. 12 shows details and numerically predicted failure mode for different types of IMF connections. FE failure modes and numerically predicted key parameters of load-displacement response at both flexural and catenary

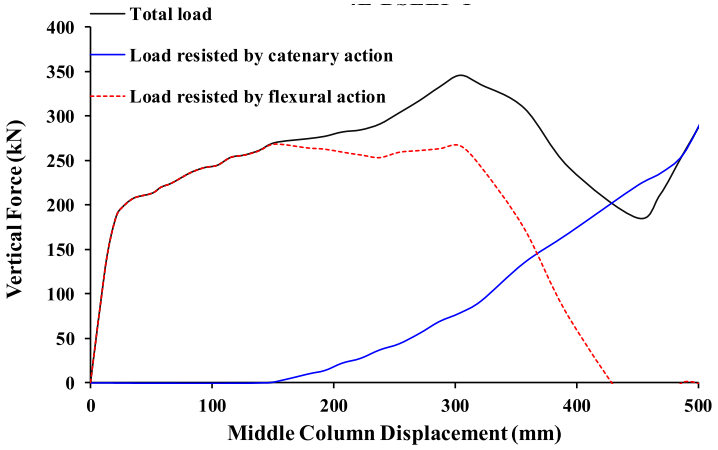

(a)

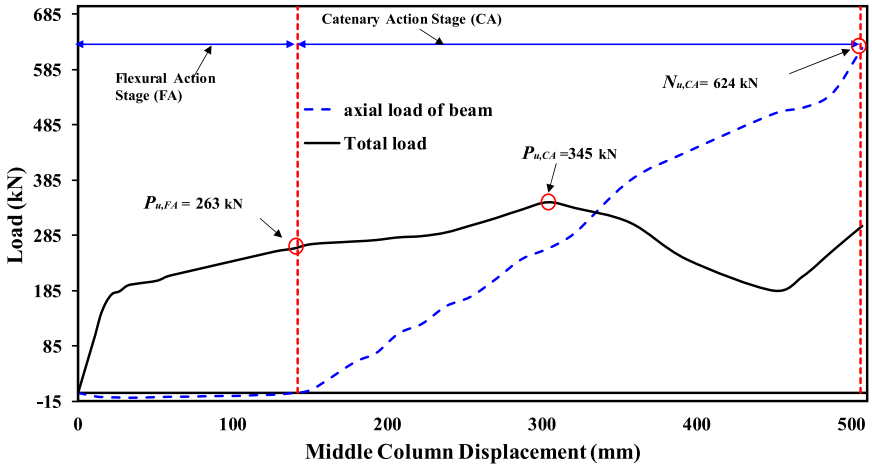

(b)

Fig. 15. FE load-displacement response for specimen 4 E-BSEEP-P: (a) Load-displacement curve; (b) Development of different action stages.

action stages are summarized in Table 5. Load versus middle column displacement curves for 7 representative samples of the 11 IMF connection specimens are displayed in Figs. 13–19. Below is a detailed discussion of the FE results for different types of IMF connections.

5.1. IMF connections in conformance with ANSI/AISC 358-16

As mentioned above, eight types of IMF beam-column connections in accordance with ANSI/AISC 358–16 [37] were studied against progressive collapse. As illustrated in Table 4, these connections, namely, are: WUF-W (welded unreinforced flange-welded web), RBS (reduced beam section), 4 E-BUEEP (bolted unstiffened extended end plate without pretensioned high-strength bolts), 4 E-BSEEP & 4 E-BSEEP-P (bolted stiffened extended end plate without and with pretensioned high-strength bolts), BFP (bolted flange plate), and KBB-W & KBB-W-P (Kaiser bolted bracket without and with pretensioned high-strength bolts).

It should be noted that WUF-W connection is the same as WUF-FW joint that has been tested in this study, but utilizes complete joint CJP groove welds to join the flanges and web of beam directly to flanges of column as shown in Fig. 12(a), thus meeting the requirements of both FEMA-350 [40] and ANSI/AISC 358–16 [37]. Load-displacement curve for WUF-W specimen is shown in Fig. 13. During the displacement controlled loading, the WUF-W connection frame underwent large rotations and displacements before its failure. At 385 mm displacement, the upper beam flange of the outer connection started to fracture and then fully detached from flange of the outer column. Subsequently, visible fracture in the shear plate occurred as seen in Fig. 12(a). At this displacement level, the load was almost 577 kN and the beam rotation was nearly 10.9° (Fig. 13).

Load displacement characteristics for RBS specimen is depicted in Fig. 14. Under controlled downward middle column displacement, the RBS connection frame underwent larger rotations and displacements than the *S*–C, WUF-FW, 4 E-BUEEP-P and WUF-W specimens before failure occurred. The RBS specimen failed at a center column displacement of about 461 mm that corresponded to beam chord rotation of about 13.0° and peak load of about 520 kN. Failure of specimen was owing to fracture of the flange in the reduced section of outer joint. As shown in Fig. 12(b), this fracture spread through the beam web till the frame could not any more take the load.

For 4 E-BSEEP and 4 E-BSEEP-P specimens which are similar to the 4 E-BUEEP but with adding end-plate stiffener and the bolts are pretensioned in specimen 4 E-BSEEP-P, there is a clear differentiation between flexural and catenary phases as shown in Fig. 15(a) and (b), which depict the load-displacement characteristics for 4 E-BSEEP-P specimen. The local deformation of the lower flange of the beam near the middle column indicated the initiation of yielding after which the second stage started with drop in the flexural stiffness. At a displacement of 142 mm,

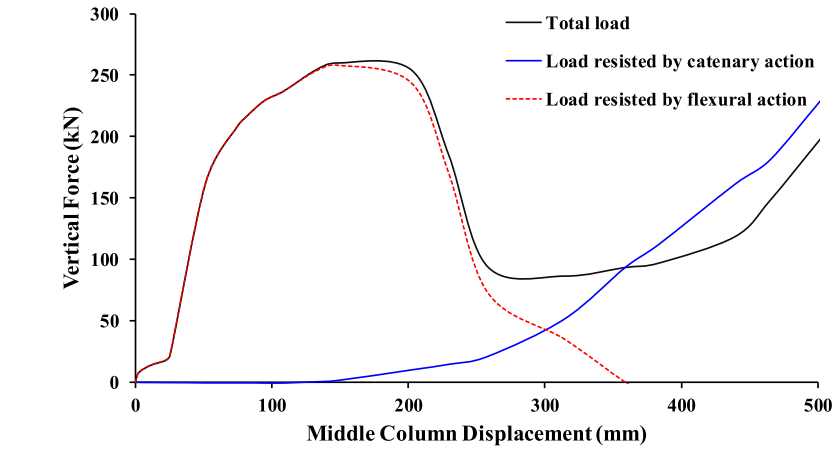

(a)

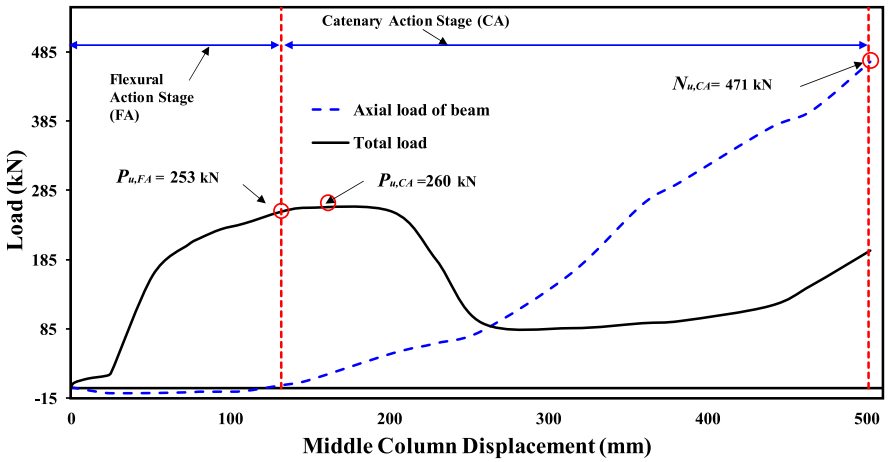

(b)

Fig. 16. FE load-displacement response for specimen BFP: (a) Load-displacement curve; (b) Development of different action stages.

the frame had its peak load of flexural action stage (263 kN). However, in the catenary action stage, peak load was 345 kN at a middle column displacement of 304 mm (see Table 5 and Fig. 15). As seen from Fig. 12 (d), the end plate and stiffener in the bottom portion of beam near middle column fractured.

Fig. 16 presents load-displacement characteristics for BFP specimen and its FE mode of failure is illustrated in Fig. 12(e). Compared with the previous connections, the bolted flange plate connection frame BFP has a reduced rotation capacity. Failure of this connection was due to shear fracture of bolts (see Fig. 12(e)), which occurred at a peak load of 260 kN (the corresponding vertical displacement was 148 mm) (see Fig. 16). At failure, the bolted flange plate has experienced substantial bearing deformation around the holes of the bolts. At small displacement levels, this connection frame could carry small load till the development of flexural and catenary actions at large displacement levels. This may be attributed to the beam-flange/top plate bolted connection. As the diameter of hole is slightly larger than the diameter of bolt, there is a small slippage between the plate and beam-flange before the bolt developing bearing against the plate and beam-flange. This may result in reduced resistance at small displacement levels as seen in Fig. 16. Subsequently, bolts developed bearing against the plate and the resistance increased at large displacement levels. This frame specimen has low vertical load resistance owing to the small rotation capacity of the connection.

Fig. 17 shows the load-displacement history of Kaiser bolted bracket with pretensioned bolts (KBB–W–P). While the bracket thickness was 20 mm and high strength bolts with 20 mm diameter were used, the weakness in the connection zone lies in the thickness of the column flange, which is 12 mm. At 120 mm displacement (the corresponding vertical load was 299 kN), the top two bolts tore some bearing material from the bolt holes and slipped from the column flange holes causing a rapid drop in resistance (see Figs. 12(f) and 17).

5.2. IMF connections in accordance with EN 1993-Eurocode 3

For the sake of comparison of progressive collapse behavior of IMF connections from different codes, the performance of two types of beam-to-column connections in accordance with EN 1993-Eurocode 3 [41] was numerically studied as seen in Table 4. These are, namely, bolted hunched joint without and with pretensioned high-strength bolts (BHJ & BHJ-P). As seen in Fig. 12(g), the connections had a 12-mm thick end plate (same as 4 E-BUEEP) and five rows of M20 class 10.9 bolts. The length and height of the haunches were 128 mm and 90 mm, respectively (Fig. 12(g)).

Load-displacement characteristics for BHJ-P specimen is shown in Fig. 18. During the initial loading phase, the performance of the

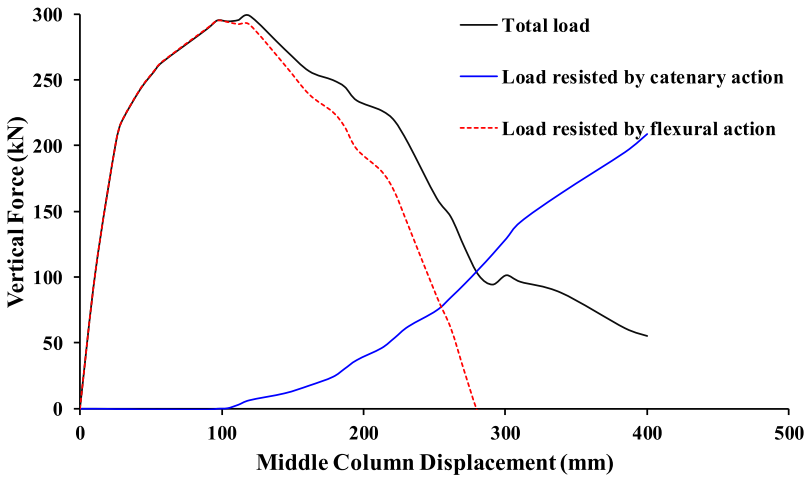

(a)

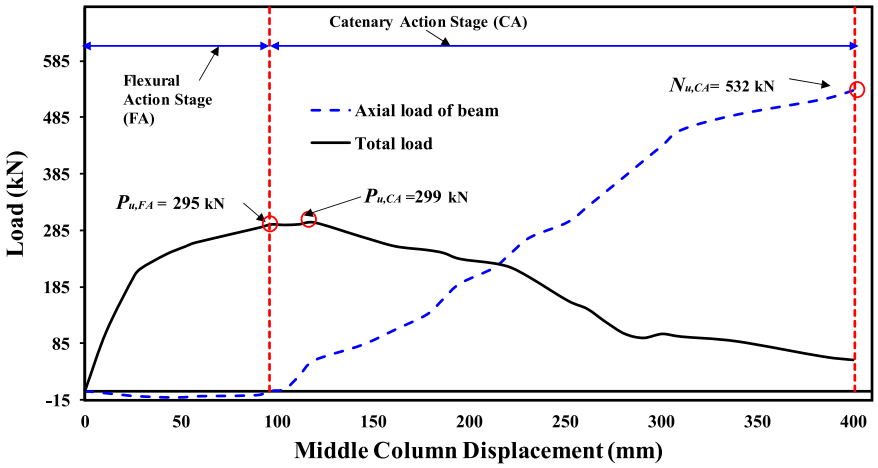

(b)

Fig. 17. FE load-displacement response for specimen KBB-W-P: (a) Load-displacement curve; (b) Development of different action stages.

connection frame was almost linear elastic without noticeable damage. After initial yielding of the beam's bottom flange near middle column had occurred, the load-displacement relationship became nonlinear with drop in the secant stiffness this stage. At middle column displacement of 137 mm, the frame had its peak load of flexural action stage (236 kN), as seen in Table 5 and Fig. 18. At vertical displacement of 137 mm, tensile axial force started to be generated in the beam indicating the onset of catenary action stage. As seen in Table 5 and Fig. 18, peak load of catenary action stage was 458 kN at a displacement of 370 mm. At this point, failure occurred in the outer joint owing to fracture of bolts as a result of the large tensile force in the beams (Fig. 12(g)).

5.3. IMF connections in accordance with TEC-2007

In addition to the IMF connections investigated previously, another type of connection in conformance with the Turkish-Earthquake-Code TEC-2007 [39] was numerically studied against progressive collapse as seen in Table 4. It is, namely, welded beam-column with joint flange plate (WJFP). This type of connection is similar in design to the FEMA 350 provisions [40]. Details of this connection are illustrated in Fig. 12 (h). The dimensions of the bottom and top cover plates of the beam flange are 140 mm long, 170 mm wide and 12 mm thick. M16 class 10.9 bolts and 6-mm shear plate are utilized to connect the beam web to the column. Load versus center column displacement curve of WJFP connection frame is displayed in Fig. 19. The frame behaved primarily in a flexural action mode before the development of catenary action stage. Up to about 20 mm displacement, the frame was kept in the elastic stage and until a displacement level of about 96 mm, the performance of the frame was dominated by flexure as indicated by the very small compressive axial force in the beam (see Fig. 19(b)). With the increase of center column displacement, tensile axial forces were generated in the beams and the behavior was controlled via catenary action. The tensile axial force in the beams kept on increasing with more middle column displacement until the connection could not any more take the combined flexural and axial stresses. At middle column displacement of 368 mm (corresponding peak load was 650 kN), failure occurred owing to fracture of the bottom cover plate close to the test column. This fracture instantly spread through the shear plate until the frame specimen could no longer carry the load as seen in Figs. 12(h) and 19.

6. Comparison of IMF connections

Fig. 20 illustrates effect of pretensioning of bolts at joints on the enhancement of response parameters of studied IMF connection

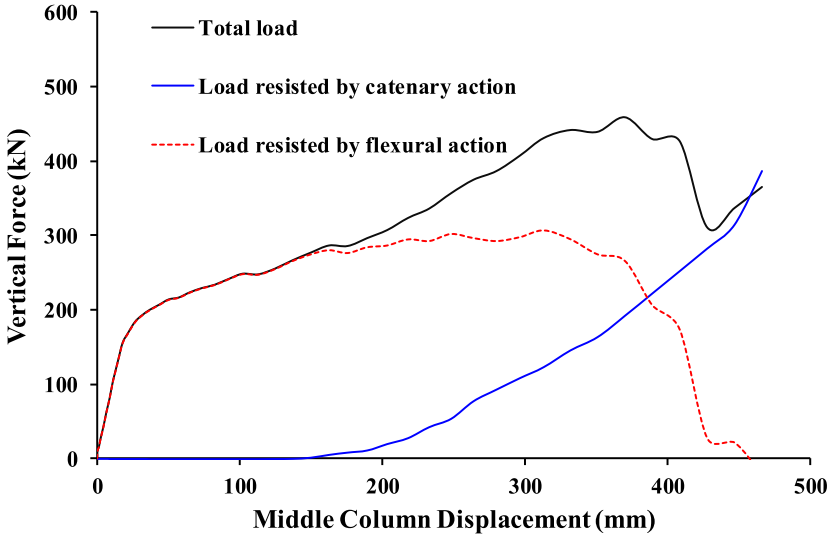

(a)

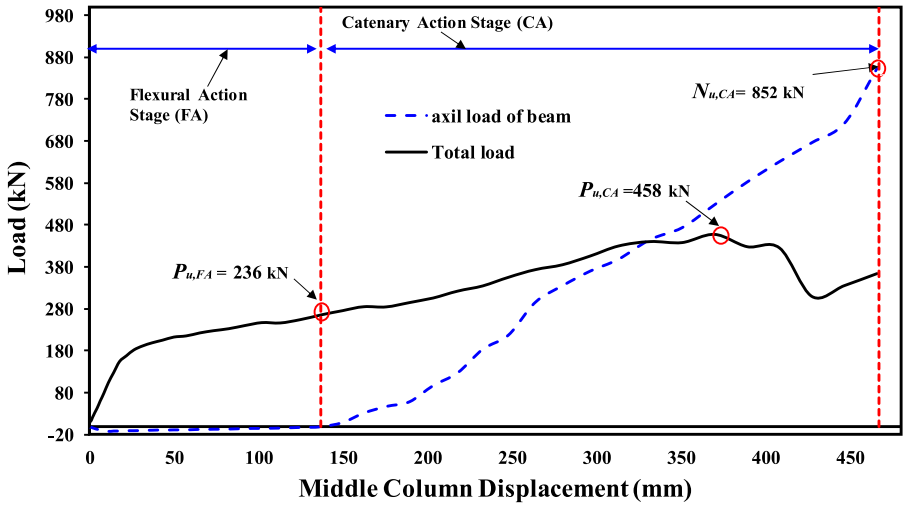

(b)

Fig. 18. FE load-displacement response for specimen BHJ-P: (a) Load-displacement curve; (b) Development of different action stages.

specimens. For pretensioned bolted connections 4 E-BUEEP-P, 4 E-BSEEP-P, KBB-W-P and BHJ-P, Fig. 20(a) and (b) depict that pre-tensioning of bolts at joints has no effect on both peak load and energy dissipation of assembly due to the complete loss of preloading between the connected parts at the peak load level as shown in Fig. 12. However, the FE results showed that bolt preloading has a limited effect on the effective stiffness of the assembly with enhancements due to pre-tensioning ranging from 5% to 11% (see Fig. 20(c)).

Table 5 shows that for all different types of connections, if axial force in beams (catenary behavior) is accounted for under a center column-missing event, the progressive collapse resistance could increase considerably, especially for frames with connections WUF-W, RBS, BHJ, BHJ-P and WJFB. If only flexural action is considered, specimens BFP, KBB-W and KBB-W-P could reach their peak load resistance without the influence of catenary action. However, for specimens 4 E-BUEEP, 4 E-BSEEP and 4 E-BSEEP-P, the catenary action has little impact on the ultimate load resistance as it enhanced the progressive collapse capacity by about 10%–30% as seen in Table 5.

Load-displacement comparison for all different types of investigated connection specimens is presented in Fig. 21. As per the experimental and FE modeling results, the studied steel beam-column connections went through three different phases of behavior (elastic stage, flexural action stage and catenary action stage). At small displacement levels of middle column, all IMF connection frames remained initially in the elastic range. In this stage, specimens WJFP and KBB-W-P have the greatest values of strength, while simple shear connection *S*–C at this stage was very weak as shown in Fig. 21. Once yielding occurred in the beam bottom flange at inner joint the second phase of response commenced and the frames resisted loads via flexural action. In the flexural action stage, specimen WJFP has the greatest load resistance followed by specimens KBB-W and KBB-W-P as seen in Table 5 and Fig. 21. For the rest of the specimens, their performance at this stage was

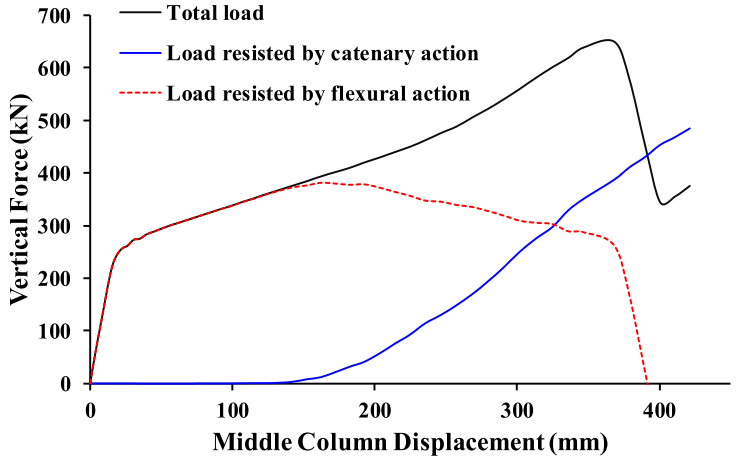

(a)

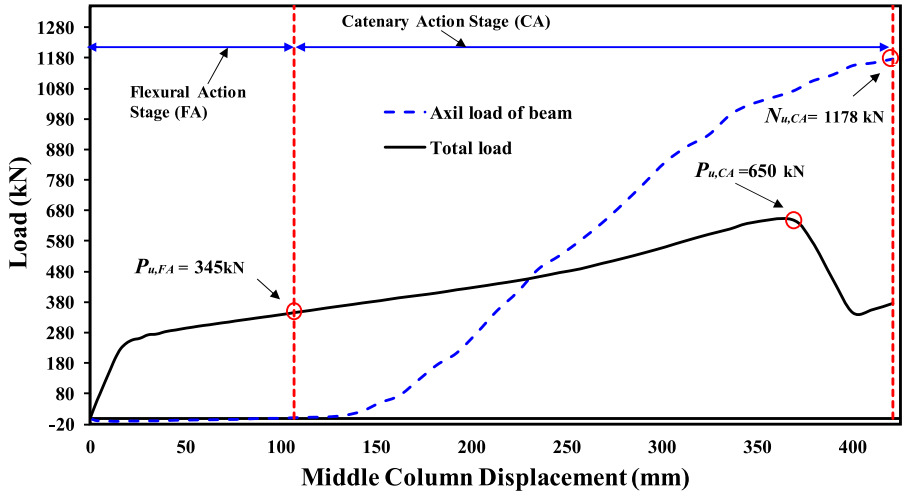

(b)

Fig. 19. FE load-displacement response for specimen WJFP: (a) Load-displacement curve; (b) Development of different action stages.

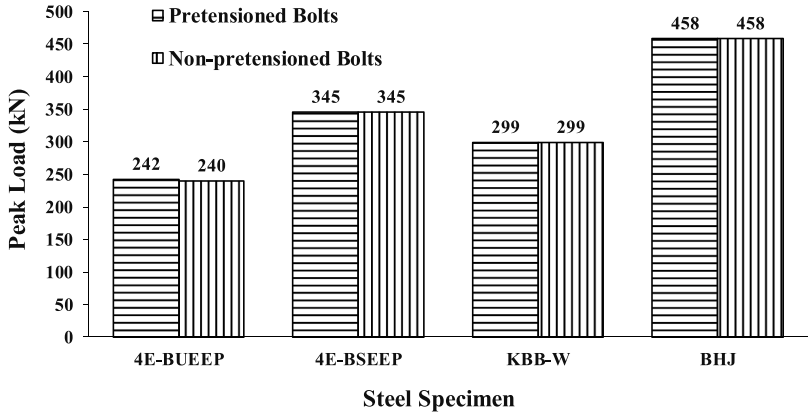

(a)

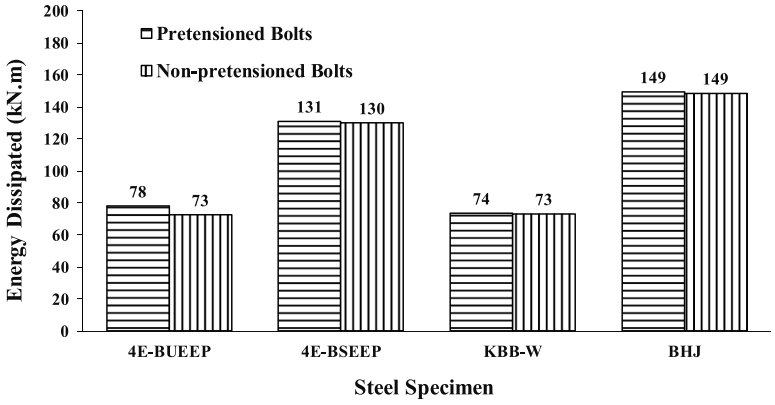

(b)

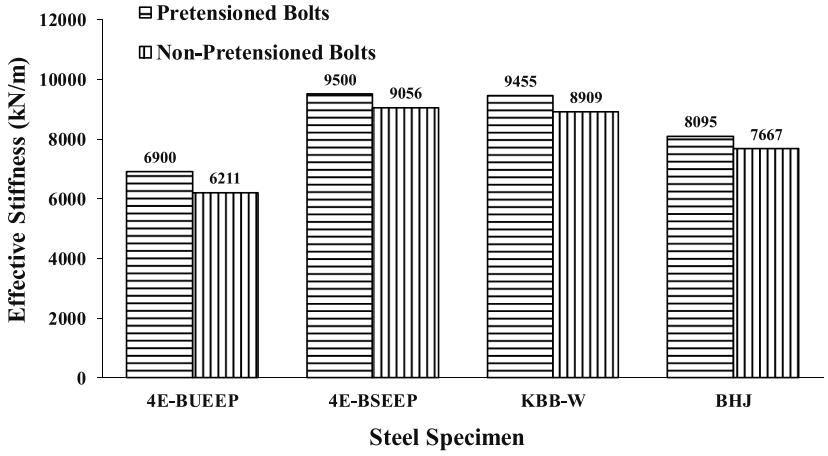

(c)

Fig. 20. Effect of pretensioning of bolts at joints on enhancement of: (a) Peak load; (b) Energy dissipated; (c) Effective stiffness.

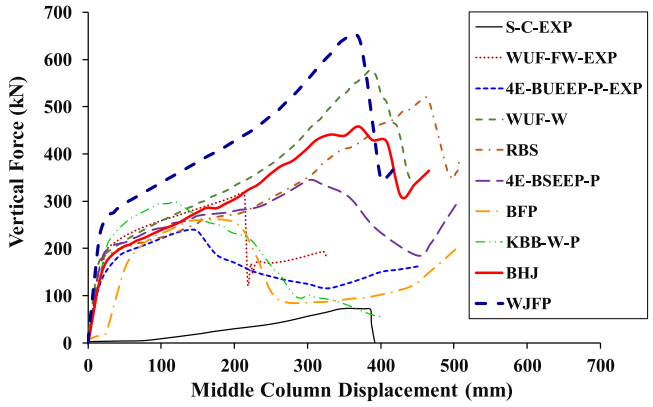

Fig. 21. Load-displacement comparison for all different types of connections.

fairly good compared to the simple shear connection specimen *S*–C. Axial tensile forces were generated in the frame beams as the middle column displacement increased, indicating development of catenary action stage. Specimens WUF-W, RBS, BHJ, BHJ-P and WJFB performed well under catenary action. For example, for specimen WJFB, Fig. 19 shows that the axial tensile force in the beam increased until the connection could not any more carry the combined axial and bending stresses.

Fig. 22 depicts a comparison of all types of connections in terms progressive collapse resistance (i.e., peak load capacity) and energy dissipated at ultimate state. Among all different types of connections, WJFP specimen, which was designed according to the Turkish-Earthquake Code TEC-2007 [39] and FEMA 350 provisions [40] had the largest progressive collapse resistance. For specimens WUF-W and RBS, even though the modes of failure are because of fracture of beam flange, they were close in the performance to WJFP connection. For specimens BHJ, BHJ-P, 4 E-BSEEP and 4 E-BSEEP-P, though the modes of failure are finally owing to bolt thread stripping or end plat fracture, failure was ductile. Prior to failure, yielding occurred in the end plate, which underwent high localized rotation and plastic deformation. This in turn developed plastic hinges into the beam-column connections and hence mobilized the catenary action stage. However, failure was brittle failure in WUF-FW, 4 E-BUEEP-P, KBB-W, KBB-W-P and BFP specimens, and the development of catenary action stage was thus limited.

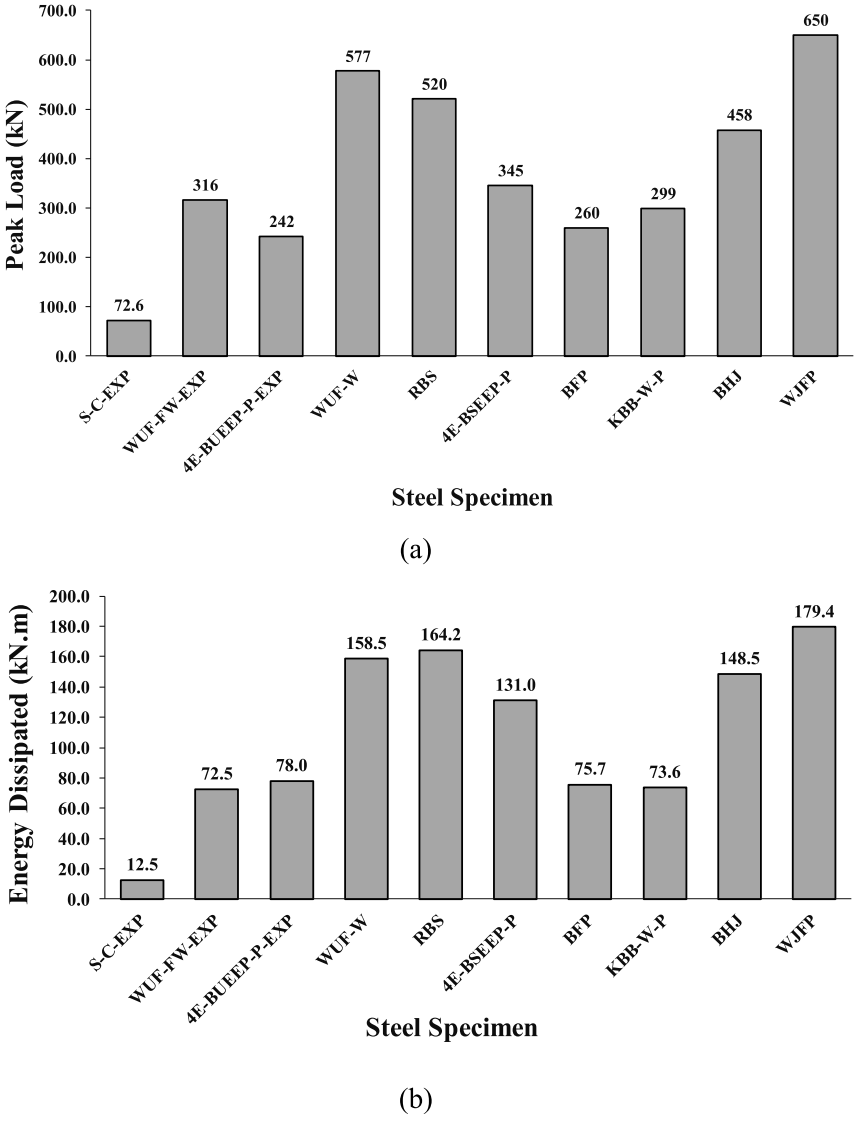

Fig. 22. Comparison of all types of connections in terms of: (a) Peak load capacity; (b) Energy dissipated.

7. Conclusions

The key findings of this research can be listed as follows:

i. The existing type of steel beam-column joint (shear connection), investigated experimentally in this research (specimen *S*–C), had a very high progressive collapse risk owing to discontinuity in the beams at joint region and hence the incapability of beams to redistribute the load carried by failed column to adjacent members.
ii. For the welded unreinforced flange-fillet welded connection investigated experimentally in this study (specimen WUF-FW), full catenary action was not mobilized and the beam axial force was considerably small due to fracture of fillet welding between bottom flange of beam and middle column. However, for the same connection with CJP groove weld at beam-to-column flanges interface (specimen WUF-W), significant axial tensile forces were generated in the beams and the catenary action stage was then fully mobilized, providing an increase in the progressive collapse resistance by about 83% more than that for specimen WUF-FW. This reveals the significance of the type of welding between beam and column flanges on the progressive collapse resistance of beam-to-column joints subjected to column-loss events.
iii. For the welded unreinforced flange-groove welded connections with or without reduced beam section (specimens WUF-W and RBS), the performance of the assembly was initially controlled by flexural action. With increased middle column displacement, large axial tensile forces were generated in the beams and the behavior at large displacement level was dominated by full development of catenary action.
iv. For pretensioned bolted connections 4 E-BUEEP-P, 4 E-BSEEP-P, KBB-W-P and BHJ-P, pretensioning of bolts at joints has no effect on both peak load and energy dissipation of assembly due to the complete loss of preloading between the connected parts at the peak load level. Yet, bolt preloading has a limited effect on the effective stiffness of the assembly with enhancements due to pretensioning ranging from 5% to 11%.
v. For both bolted stiffened extended end-plate connections (4 E-BSEEP and 4 E-BSEEP-P) and connections in conformance with EN 1993-Eurocode 3 [38] (BHJ and BHJ-P), even though the failure modes are due to bolt thread stripping or end plate and stiffener fracture, failure was ductile with increased dissipated energy at ultimate state. Prior to failure, yielding occurred in the end plate, which underwent high localized rotation and plastic deformation. This in turn developed plastic hinges into the beam-column connections and hence mobilized the catenary action stage.
vi. None of BFP, KBB-W and KBB-W-P connections developed significant catenary action and therefore, these connections had limited ductility and dissipated energy at ultimate state as compared to other IMF connections. They may be useful only for small displacement with flexural action.
vii. Among all different types of studied connections, WJFP specimen, which was designed according to the Turkish-Earthquake Code TEC-2007 [39] and FEMA 350 provisions [40] had the largest progressive collapse resistance. This type of connection increased the progressive collapse resistance significantly to almost 9 times of that for control shear connection frame *S*–C.

Declaration of competing interest

The authors declare that they have no known competing financial interests or personal relationships that could have appeared to influence the work reported in this paper.

Acknowledgement

The authors are grateful to the Deanship of Scientific Research, King Saud University, for funding through Vice Deanship of Scientific Research Chairs.

Appendix A. Supplementary data

Supplementary data to this article can be found online at https://doi.org/10.1016/j.tws.2020.106875.

References

[1] W. McGuire, Prevention of progressive collapse, Proc. Regional Conf. on Tall Buildings (1974). Bangkok, Thailand.
[2] E.V. Leyendecker, B.R. Ellingwood, Design Methods for Reducing the Risk of Progressive Collapse in Buildings, National Bureau of Standards, Washington, DC, 1977.
[3] W.G. Corley, P.F. Mlakar, M.A. Sozen, C.H. Thornton, The Oklahoma City bombing: Summary and recommendations for multihazard mitigation, J. Perform. Constr. Facil. 12 (3) (1998) 100–112.
[4] Z.P. Bazant, Y. Zhou, Why did the world trade center collapse?-simple analysis, J. Eng. Mech. 128 (1) (2002) 2–6.
[5] Z.P. Bazant, M. Verdure, Mechanics of progressive collapse: learning from world trade center and building demolitions, J. Eng. Mech. 133 (3) (2007) 308–319.
[6] Z.P. Bazant, J. Le, F.R. Greening, D.B. Benson, What did and did not cause collapse of world trade center twin towers in New York, J. Eng. Mech. 134 (10) (2008) 892–906.
[7] K.A. Seffen, Progressive collapse of the world trade center: simple analysis, J. Eng. Mech. 134 (2) (2008) 125–132.
[8] S. Marjanishvili, E. Agnew, Comparison of various procedures for progressive collapse analysis, J. Perform. Constr. Facil. 20 (4) (2006) 365–374.
[9] F. Fu, Progressive collapse analysis of high-rise building with 3-D finite element modeling method, J. Constr. Steel Res. 65 (2009) 1269–1278.
[10] K. Khandelwal, S. El-Tawil, F. Sadek, Progressive collapse analysis of seismically designed steel braced frames, J. Constr. Steel Res. 65 (2009) 699–708.
[11] J. Kim, T. Kim, Assessment of progressive collapse-resisting capacity of steel moment frames, J. Constr. Steel Res. 65 (2009) 169–179.
[12] J. Kim, D. An, Evaluation of progressive collapse potential of steel moment frames considering catenary action, Struct. Des. Tall Special Build. 18 (2009) 455–465.
[13] D. Grierson, M. Safi, L. Xu, Y. Liu, Simplified methods for progressive-collapse analysis of buildings, in: Proc. Metropolis and beyond, Structures Congress, Reston, VA, 2005.
[14] B.A. Izzuddin, A.G. Vlassis, A.Y. Elghazouli, D.A. Nethercot, Progressive collapse of multistory buildings due to sudden column loss. Part I: simplified assessment framework, Eng. Struct. 30 (2008) 1308–1318.
[15] A.G. Vlassis, B.A. Izzuddin, A.Y. Elghazouli, D.A. Nethercot, Progressive collapse of multistorey buildings due to sudden column loss—Part II: Application, Eng. Struct. 30 (2008) 1424–1438.
[16] C. Lee, S. Kim, K. Han, K. Lee, Simplified nonlinear progressive collapse analysis of welded steel moment frames, J. Constr. Steel Res. 65 (2009) 1130–1137.
[17] A. Naji, F. Irani, Progressive collapse analysis of steel frames: simplified procedure and explicit expression for dynamic increase factor, Int J Steel Struct 12 (4) (2012) 537–549.
[18] H.M. Elsanadedy, T.H. Almusallam, Y.R. Alharbi, Y.A. Al-Salloum, H. Abbas, Progressive collapse potential of a typical steel building due to blast attacks, J. Constr. Steel Res. 101 (2014) 143–157.
[19] Livermore Software Technology Corporation (Lstc), LS-DYNA User's Keyword Manual (Nonlinear Dynamic Analysis of Structures in Three Dimensions), vol. 1, LSTC, Livermore, California, 2007. Version 971.
[20] A. Hadidi, R. Jasour, A. Rafiee, On the progressive collapse resistant optimal seismic design of steel frames, Struct. Eng. Mech. 60 (5) (2016) 761–779.
[21] ANSI/AISC 360-05, Specifications for Structural Steel Buildings, American Institute of Steel Construction, Chicago, IL, USA, 2005.
[22] US Department of Defense (DoD), Unified Facilities Criteria (UFC), DoD Minimum Antiterrorism Standards for Buildings, US Army Corps of Engineering, Washington, DC: Department of Defense, 2002, p. 31. UFC 4-010-01.
[23] M. Mirtaheri, M.A. Zoghi, Design guides to resist progressive collapse for steel structures, Steel Compos. Struct. 20 (2) (2016) 357–378.
[24] M.A. Zoghi, M. Mirtaheri, Progressive collapse analysis of steel building considering effects of infill panels, Struct. Eng. Mech. 59 (1) (2016) 59–82.
[25] C.H. Chen, Y.F. Zhu, Y. Yao, Y. Huang, Progressive collapse analysis of steel frame structure based on the energy principle, Steel Compos. Struct. 21 (3) (2016) 553–571.
[26] H. Abbas, N. Jones, Influence of strain hardening on bending moment–axial force interaction, Int. J. Mech. Sci. 55 (1) (2012) 65–77.
[27] M. Hosseini, H. Abbas, Strain hardening in M–P interaction for metallic beam of I-section, Thin-Walled Struct. 62 (2013) 243–256.
[28] S.W. Bae, R.A. LaBoube, A. Belarbi, A. Ayoub, Progressive collapse of cold-formed steel framed structures, Thin-Walled Struct. 46 (7–9) (2008) 706–719.
[29] Q. Han, X. Li, M. Liu, B.F. Spencer Jr., Performance analysis and macromodel simulation of steel frame structures with beam-column joints using cast steel

stiffeners for progressive collapse prevention, Thin-Walled Struct. 140 (2019) 404–415.
[30] H.S. Lew, J.A. Main, S.D. Robert, F. Sadek, V.P. Chiarito, Performance of steel moment connections under a column removal scenario. I: Experiments, J Struct Eng-ASCE 139 (1) (2013) 98–107.
[31] Y. Gong, Test, modeling and design of bolted-angle connections subjected to column removal, J. Constr. Steel Res. 139 (2017) 315–326.
[32] C. Liu, K.H. Tan, T.C. Fung, Dynamic behaviour of web cleat connections subjected to sudden column removal scenario, J. Constr. Steel Res. 86 (2013) 92–106.
[33] W. Wang, L. Li, D. Chen, Progressive collapse behaviour of endplate connections to cold-formed tubular column with novel Slip-Critical Blind Bolts, Thin-Walled Struct. 131 (2018) 404–416.
[34] B. Yang, K.H. Tan, Experimental tests of different types of bolted steel beam–column joints under a central-column-removal scenario, Eng. Struct. 54 (2013) 112–130.
[35] B. Yang, K.H. Tan, Numerical analyses of steel beam–column joints subjected to catenary action, J. Constr. Steel Res. 70 (2012) 1–11. .
[36] F. Dinu, I. Marginean, D. Dubina, Experimental testing and numerical modelling of steel moment-frame connections under column loss, Eng. Struct. 151 (2017) 861–878. .
[37] ANSI/AISC 358-16, Prequalified Connections for Special and Intermediate Steel Moment Frames for Seismic Applications, American Institute of Steel Construction, Chicago, IL, USA, 2016.
[38] E.N. CEN, 1993-1-5 Eurocode 3: Design of Steel Structures - Part 1-5, General rules - Plated structural elements, Brussels, 2006.
[39] TEC-, Specification for Buildings to Be Built in Disaster Areas, Ministry of Public Works and Settlement, Ankara, Turkey, 2007, 2007.
[40] SAC Joint Venture, Guidelines Development Committee, et al, in: Recommended Seismic Design Criteria for New Steel Moment-Frame Buildings, vol. 350, Federal Emergency Management Agency (FEMA), 2000, p. .
[41] S. Gerasimidis, Analytical assessment of steel frames progressive collapse vulnerability to corner column loss, J. Constr. Steel Res. 95 (2014 4 1) 1–9.
[42] P. Pantidis, S. Gerasimidis, New Euler-type progressive collapse curves for steel moment-resisting frames: analytical method, J. Struct. Eng. 143 (9) (2018 9 1), 04017113.
[43] M. Ettouney, R. Smilowitz, M. Tang, A. HapijGlobal system considerations for progressive collapse with extensions to other natural and man-made hazards, J. Perform. Constr. Facil. ASCE 20 (4) (2006 11) 403–417.
[44] S. Gerasimidis, G. Deodatis, T. Kontoroupi, M. Ettouney, Loss-of-stability induced progressive collapse modes in 3D steel moment frames, Struct. Infrastruct. Eng. 11 (3) (2015 3 4) 334–344.
[45] K. Khandelwal, S. El-Tawil, Pushdown resistance as a measure of robustness in progressive collapse analysis, J. Struct. Eng. 33 (9) (2011 9 1) 2653–2661.
[46] D.Y. Kong, Y. Yang, B. Yang, X.H. Zhou, Experimental study on progressive collapse of 3D steel frames under concentrated and uniformly distributed loading conditions, J. Struct. Eng. 146 (4) (2020 4 1), 04020017.
[47] Abaqus 6.17 Analysis User's Guide, Section 12.9.3 – Defining Damages, Dassault Systemes Simulia Corp., Providence, RI, 2017.
[48] ANSI/AISC 360-16, Specifications for Structural Steel Buildings, American Institute of Steel Construction, Chicago, IL, USA, 2016.
[49] ASTM, Standard Specification for High-Strength Steel Bolts, Classes 10.9 and 10.9.3, for Structural Steel Joints (Metric). ASTM A490M-14, American Society for Testing and Materials, West Conshohocken, PA, USA, 2014.
[50] H. Tang, X. Deng, Y. Jia, J. Xiong, C. Peng, Study on the progressive collapse behavior of fully bolted RCS beam-to-column connections, Eng. Struct. 199 (2019) 109618.
[51] T. Almusallam, Y. Al-Salloum, H. Elsanadedy, N. Tuan, P. Mendis, H. Abbas, Development limitations of compressive arch and catenary actions in reinforced concrete special moment resisting frames under column-loss scenarios, Struct Infrastruct E (2020) 1–19.
[52] H.M. Elsanadedy, T.H. Almusallam, Y.A. Al-Salloum, H. Abbas, Investigation of precast RC beam-column assemblies under column-loss scenario, Construct. Build. Mater. 142 (2017) 552–571. .
[53] Y.A. Al-Salloum, M.A. Alrubaidi, H.M. Elsanadedy, T.H. Almusallam, R.A. Iqbal, Strengthening of precast RC beam-column connections for progressive collapse mitigation using bolted steel plates, Eng. Struct. 161 (2018) 146–160.
[54] New Zealand Standard (NZS), Code of Practice for General Structural Design and Design Loadings for Buildings 1, NZS 4203, 1992 (New Zealand).
[55] B. Meng, W. Zhong, J. Hao, Anti-collapse performances of steel beam-to-column assemblies with different span ratios, J. Constr. Steel Res. 140 (2018) 125–138.
[56] ASTM, Standard Test Methods and Definitions for Mechanical Testing of Steel Products, American Society for Testing and Materials, West Conshohocken, PA, USA, 2016. ASTM A370 - 16.
[57] Y. Bao, T. Wierzbicki, On fracture locus in the equivalent strain and stress triaxiality space, Int. J. Mech. Sci. 46 (1) (2004) 81–98. .
[58] P. Arasaratnam, K.S. Sivakumaran, M.J. Tait, True stress-true strain models for structural steel elements, ISRN Civil Engineering (2011) 11. Article ID 656401.
[59] W. Wang, C. Fang, X. Qin, Y. Chen, L. Li, Performance of practical beam-to-SHS column connections against progressive collapse, Eng. Struct. 106 (2016) 332–347.